Stem Cell Reports
Article

ISSCR

OPEN ACCESS

SFRP1 in Skin Tumor Initiation and Cancer Stem Cell Regulation with Potential Implications in Epithelial Cancers

Raghava R. Sunkara,[1,4] Rahul M. Sarate,[1] Priyanka Setia,[1] Sanket Shah,[2,4] Sanjay Gupta,[2,4] Pankaj Chaturvedi,[3] Poonam Gera,[5] and Sanjeev K. Waghmare[1,4,*]

[1]Stem Cell Biology Group, Waghmare Lab, Cancer Research Institute, Advanced Centre for Treatment Research and Education in Cancer (ACTREC), Tata Memorial Centre, Kharghar, Navi Mumbai, Maharashtra 410210, India
[2]Epigenetics and Chromatin Biology Group, Gupta Lab, Cancer Research Institute, Advanced Centre for Treatment Research and Education in Cancer (ACTREC), Tata Memorial Centre, Kharghar, Navi Mumbai, Maharashtra 410210, India
[3]Tata Memorial Hospital, Parel, Mumbai, India
[4]Homi Bhabha National Institute, Training School Complex, Anushakti Nagar, Mumbai 400085, India
[5]Cancer Research Institute, ACTREC, Tata Memorial Centre, Kharghar, Navi Mumbai, Maharashtra 410210, India
*Correspondence: swaghmare@actrec.gov.in
https://doi.org/10.1016/j.stemcr.2019.12.006

SUMMARY

Wnt signaling is involved in the regulation of cancer stem cells (CSCs); however, the molecular mechanism involved is still obscure. *SFRP1*, a Wnt inhibitor, is downregulated in various human cancers; however, its role in tumor initiation and CSC regulation remains unexplored. Here, we used a skin carcinogenesis model, which showed early tumor initiation in *Sfrp1*$^{-/-}$ (*Sfrp1* knockout) mice and increased tumorigenic potential of *Sfrp1*$^{-/-}$ CSCs. Expression profiling on *Sfrp1*$^{-/-}$ CSCs showed upregulation of genes involved in epithelial to mesenchymal transition, stemness, proliferation, and metastasis. Further, *SOX-2* and *SFRP1* expression was validated in human skin cutaneous squamous cell carcinoma, head and neck squamous cell carcinoma, and breast cancer. The data showed downregulation of *SFRP1* and upregulation of *SOX-2*, establishing their inverse correlation. Importantly, we broadly uncover an inverse correlation of *SFRP1* and *SOX-2* in epithelial cancers that may be used as a potential prognostic marker in the management of cancer.

INTRODUCTION

Cancer is a heterogeneous disease at both the cellular and the molecular level. The heterogeneity arises from the number of events, including genetic, epigenetic, and transcriptional alterations (Latil et al., 2017). Within the tumor, a subset of cells possesses an unlimited self-renewal activity, higher tumorigenic potential, and resistance to conventional therapies, termed as cancer stem cells (CSCs) (Batlle and Clevers, 2017). CSCs have been isolated from various cancers such as leukemia, breast cancer, head and neck cancers, etc. (Al-Hajj et al., 2003; Bonnet and Dick, 1997; Prince et al., 2007). These CSCs escape chemoradiotherapy thereby leading to recurrence of the tumor followed by metastasis (Nassar and Blanpain, 2016). During the process of epithelial to mesenchymal transition (EMT), epithelial cells lose their properties and acquire the mesenchymal fate, which confers on the cells migratory and invasive properties (Thiery et al., 2009). Although the EMT process is activated during embryonic development for the formation and differentiation of various tissues and organs, its activity in cancer cells was reported to endow stem cell-like properties. Recent findings have shown that the overexpression of EMT markers such as *TWIST1*, *SNAIL*, *ZEB1*, etc., in cancer cells converts them to cancer stem-like cells (Morel et al., 2008; Wellner et al., 2009). Thus, this suggests that there may be a link between the EMT and CSCs. Further, developmental signaling pathways, such as Wnt, Sonic hedgehog, Notch, etc., are involved in the regulation of EMT and CSCs (Karamboulas and Ailles, 2013).

Wnt signaling is involved in self-renewal, cell fate determination, migration, polarity, etc., during both embryonic development and adult tissue homeostasis (Clevers, 2006; Steinhart and Angers, 2018). Wnt signaling is tightly regulated by various secreted antagonists such as secretory frizzled-related proteins (SFRPs), Wnt inhibitory factor-1, and Dickkopf proteins (Kawano and Kypta, 2003). Moreover, intracellular noncanonical Wnt pathways were shown to regulate the canonical Wnt pathway by inhibiting β-catenin (Renstrom et al., 2009). SFRPs are a family of natural Wnt inhibitors that are present in the extracellular compartment, which inhibits Wnt signaling, and are also involved in embryonic development and tissue homeostasis (Matsuyama et al., 2009). Further, *Sfrp1* is upregulated in the hair follicle stem cells (HFSCs) (Lien et al., 2011; Tumbar et al., 2004), while it is downregulated in various cancers. In oral squamous cell carcinoma (OSCC), silencing of the *SFRP1*, *SFRP2*, and *SFRP5* genes was observed, due to methylation, in both oral cancer cell lines and tumor specimens (Sogabe et al., 2008). Further, methylation of the *SFRP1* promoter was observed in esophageal squamous cell carcinoma (Meng et al., 2011) and hepatocellular carcinoma (Davaadorj et al., 2016). *SFRP1* loss was also observed in invasive breast cancer tissues and cell lines through either gene deletion or promoter

hypermethylation (Bernemann et al., 2014; Veeck et al., 2006). In addition, *SFRP* (1, 2, 4, and 5) gene promoters are hypermethylated in cutaneous squamous cell carcinoma (SCC) in Chinese patient samples (Liang et al., 2015). Moreover, microRNAs such as miR-1301-3p negatively target *GSK-3β* and *SFRP1*, and promote the expansion of CSCs in prostate cancer (Song et al., 2018). Although *SFRP1* was shown to be lost in multiple epithelial cancers, including skin, OSCC, and breast cancers, its role in tumor initiation and CSC regulation is still obscure. Interestingly, epithelial tissues such as epidermis, oral epithelium, and breast epithelium have been reported to have similarities in tissue architecture and function as well as during tumor progression and metastasis.

Epidermis and oral epithelium are made up of stratified squamous epithelial layers consisting of stratum basale, stratum spinosum, stratum granulosum, and stratum corneum (gingiva and hard palate) (Muroyama and Lechler, 2012; Porcheri et al., 2019). Optimum levels of Wnt signaling are essential for the maintenance and differentiation of both skin and oral epithelia (Lim and Nusse, 2013; Liu and Millar, 2010). Further, Notch signaling drives the differentiation of keratin 5/14-positive basal epithelial cells into keratin 1/10-positive suprabasal cells in skin as well as oral epithelium (Blanpain et al., 2006; Porcheri et al., 2019). Moreover, both tissues express similar kinds of integrins, such as α2β1, α3β1, and α6β4 (in the basal layer) (Larjava et al., 2011; Owens et al., 2003), and terminal differentiation markers such as filaggrin (in the stratum corneum layer of the epidermis and gingiva/hard palate) (De Benedetto et al., 2008; Presland and Dale, 2000). Similarly, breast epithelium also has stratified epithelial organization and consists of basal/myoepithelial cells and luminal cells (Huebner et al., 2014). Importantly, Wnt/β-catenin is involved in the maintenance of basal/myoepithelial cells inhibiting luminal differentiation (Gu et al., 2013). Similar to that of skin, Notch signaling also plays a significant role in the differentiation and stratification of breast epithelium (Regan et al., 2013). The basal/myoepithelial cells also express keratins such as K5 and K14, which are characteristic of the basal layer of stratified epithelia. Further, integrins such as α2β1, α3β1, and α6β4 are also expressed in the basal layer of breast epithelium similar to that of epidermis (Faraldo et al., 2005).

Interestingly, the epithelial tissues also show certain similarities even in tumor progression and metastasis. For instance, head and neck SCC (HNSCC), triple-negative breast cancer (TNBC), and cutaneous SCC overexpress epidermal growth factor receptor, which plays an important role in tumor progression and metastasis (Argiris, 2015; Liao et al., 2019; Uribe and Gonzalez, 2011). Further, Keratin-8, a marker for more invasive and undifferentiated skin SCC (Caulin et al., 1993), is also a known marker for poor prognosis in OSCC (Fillies et al., 2006). In addition, upregulation of α5β6 integrin and matrix metalloprotease-9 promotes invasion and metastasis in basal cell carcinoma of skin, OSCC, and breast cancers (Arihiro et al., 2000; Lu et al., 2008; Ramos et al., 2002). Significantly, *SFRP1* loss due to hypermethylation is reported in skin cutaneous SCC (Liang et al., 2015), breast cancer (Veeck et al., 2006), and OSCC (Sogabe et al., 2008). Therefore, owing to the similarity among epithelial tissues at both the tissue and the tumor levels, the information gained from the studies on skin cancer can be extrapolated to other epithelial cancers such as HNSCC and breast cancers.

In the present study, we show that the loss of *Sfrp1* in mouse skin leads to early tumor initiation with an early formation of papillomas and SCC. CSCs isolated from *Sfrp1*$^{-/-}$ tumors showed increased *in vivo* tumorigenic potential with enhanced tumor propagating cell (TPC) frequency. Importantly, the expression profile on the CSCs of *Sfrp1*$^{-/-}$ tumors showed an upregulation of genes involved in the regulation of tumor aggressiveness, metastasis (EMT markers), and stemness (*Sox-2*). Further, we extrapolated our data from mouse to human epithelial cancers and checked for the expression pattern of *SFRP1* and *SOX-2* in skin cutaneous SCC, HNSCC (OSCC samples), and breast cancer. The results showed *SFRP1* was downregulated, whereas *SOX-2* was upregulated in all three cancers, establishing an inverse correlation of *SFRP1* and *SOX-2* in these cancers. Importantly, within the TCGA database, *SFRP1* downregulation is associated with increased *SOX-2* expression and overall poor survival in multiple epithelial cancers.

RESULTS

Sfrp1 Loss Results in Accelerated Tumor Initiation with Chemical-Induced Carcinogenesis

To delineate the role of *Sfrp1* in tumor initiation, we used the 7,12-dimethylbenz[a]anthracene (DMBA)/12-O-tetradecanoyl phorbol-13-acetate (TPA)-induced skin carcinogenesis protocol as mentioned in the Experimental Procedures. The wild type (WT), *Sfrp1*$^{+/-}$ (heterozygous knockout), and *Sfrp1*$^{-/-}$ (homozygous knockout) mice were treated with DMBA and TPA at various postnatal days as shown in the schematic (Figure 1A). *Sfrp1*$^{-/-}$ mice showed an early papilloma formation after 10–12 weeks of TPA treatment (Figure 1B), while the *Sfrp1*$^{+/-}$ mice showed papilloma formation after 12–14 weeks, compared with the WT mice that showed at 16–18 weeks posttreatment. Thus, the study demonstrated that in *Sfrp1*$^{-/-}$ and *Sfrp1*$^{+/-}$ mice papilloma formation appears earlier by 3–4 weeks and 2–3 weeks, respectively, compared with WT mice (Figures 1C–1E). Further, we counted the average

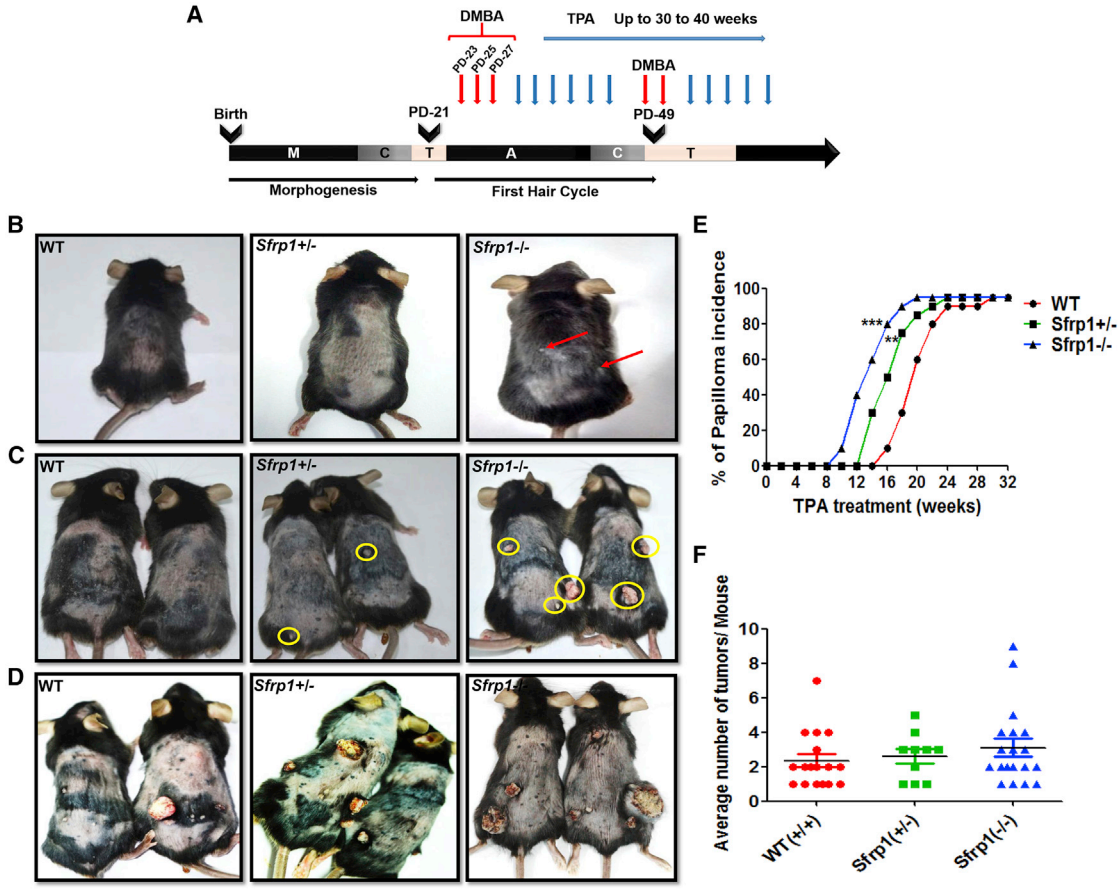

Figure 1. *Sfrp1* Loss Accelerates Tumor Initiation and SCC Progression

(A) Schematic representation for two-step chemical-induced carcinogenesis using DMBA/TPA.

(B) WT, *Sfrp1*$^{+/-}$, and *Sfrp1*$^{-/-}$ mice showing difference in tumor formation after 12 weeks of TPA application. Red arrows show papilloma formation in *Sfrp1*$^{-/-}$ mice.

(C) WT, *Sfrp1*$^{+/-}$, and *Sfrp1*$^{-/-}$ mice showing difference in tumor formation after 18 weeks of TPA application. Yellow circles show papilloma formation in *Sfrp1*$^{+/-}$ and *Sfrp1*$^{-/-}$ mice.

(D) WT, *Sfrp1*$^{+/-}$, and *Sfrp1*$^{-/-}$ mice showing difference in tumor formation after 25 weeks of TPA application.

(E) Graph depicting percentage of papilloma incidence versus TPA application in weeks, in WT, *Sfrp1*$^{+/-}$, and *Sfrp1*$^{-/-}$, mice (n = 11 mice/genotype).

(F) Graph depicting average number of tumors per mouse in WT, *Sfrp1*$^{+/-}$, and *Sfrp1*$^{-/-}$ mice (n = 17 for WT, n = 10 for *Sfrp1*$^{+/-}$, and n = 19 for *Sfrp1*$^{-/-}$).

WT, wild type; *Sfrp1*$^{+/-}$, heterozygous for *Sfrp1*; *Sfrp1*$^{-/-}$, homozygous knockout for *Sfrp1*; DMBA, 7,12-dimethylbenz[a]anthracene; TPA, 12-O-tetradecanoyl phorbol-13-acetate; A, anagen; C, catagen; T, telogen; M, morphogenesis; SCC, squamous cell carcinoma. Data were analyzed by Student's t test and presented as means ± SEM. **p < 0.01, ***p < 0.001. See also Figure S1.

number of tumors per mouse in the *Sfrp1*$^{-/-}$ and *Sfrp1*$^{+/-}$ mice compared with WT mice. Although loss of *Sfrp1* showed an early tumor initiation, it does not have any effect on the tumor burden (Figure 1F). Hematoxylin and eosin (H&E) staining showed that the *Sfrp1*$^{-/-}$ SCCs mostly had the mixed phenotype (tumor containing both epithelial cells and mesenchymal cells), while a few SCCs showed a mesenchymal phenotype. In WT tumors, the SCCs mostly showed a well-differentiated epithelial phenotype and a few SCCs showed a mixed phenotype (Figure S1). Further, we performed an immunofluorescence assay (IFA) using Ki-67 (proliferation marker) and K5 and α6-integrin (basal epithelial markers) in the papillomas of the WT and *Sfrp1*$^{-/-}$ mice. Our results showed no change in proliferation or in the expression of basal epithelial markers (Figures 2A and 2B). Hence, our results suggest that *Sfrp1*$^{-/-}$ mice showed accelerated tumor initiation and also the tumors were primarily of mixed phenotype compared with the epithelial phenotype of WT tumors.

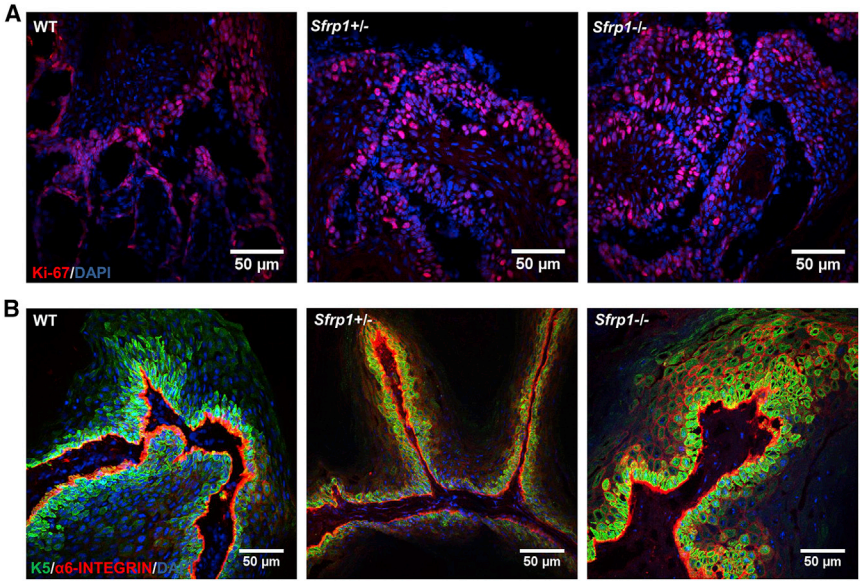

Figure 2. Characterization of WT, *Sfrp1*$^{+/-}$, and *Sfrp1*$^{-/-}$ Mouse Papillomas

Immunofluorescence analysis of (A) Ki-67 and (B) keratin 5 (K5) and α6-integrin expression on 7 μm thick cryosections in WT, *Sfrp1*$^{+/-}$, and *Sfrp1*$^{-/-}$ mouse papillomas (n = 4 biological replicates/genotype).

WT, wild type; *Sfrp1*$^{+/-}$, heterozygous for *Sfrp1*; *Sfrp1*$^{-/-}$, homozygous knockout for *Sfrp1*; scale bar: 50 μm.

CSCs of *Sfrp1* Knockout Tumors Possess Higher Tumorigenic Potential

Sfrp1 loss showed accelerated tumor initiation; hence, we further investigated its involvement in CSC regulation. In this regard, we performed flow cytometry to analyze the CSCs from the *Sfrp1*$^{-/-}$ SCCs and WT SCCs, by using well-defined CSC markers (Lin^{-}/Epcam^{+}/α6-integrin^{+}/CD34^{+}) for skin SCC. The results showed that there was no alteration in the percentage of the CSCs in the WT and *Sfrp1*$^{-/-}$ mouse skin SCC (Figure 3A). Further, we performed an *in vivo* tumorigenic potential assay using fluorescence-activated cell sorting (FACS)-sorted CSCs from both the *Sfrp1*$^{-/-}$ SCCs and WT SCCs by subcutaneously transplanting 20,000 CSCs into NOD/SCID mice. The results showed that the *Sfrp1*$^{-/-}$ CSCs are able to give rise to tumor after 2–3 weeks of injection, but WT CSCs required 5–6 weeks for the tumor formation (Figures 3B and 3C). In addition, we also performed a serial transplantation assay of CSCs, which is the gold standard assay to determine the presence of CSCs. The results showed that FACS-sorted cells are indeed CSCs, which showed high tumorigenic potential when transplanted into NOD/SCID mice. In addition, 20,000 CSCs isolated from *Sfrp1*$^{-/-}$ primary tumors, when transplanted into NOD/SCID mice, showed tumor formation (secondary tumors) within 3 weeks. Subsequently, 20,000 CSCs from the *Sfrp1*$^{-/-}$ secondary tumors, when transplanted into NOD/SCID mice, showed tumors (tertiary tumors) within 10–14 days. This suggests that the CSCs from the *Sfrp1*$^{-/-}$ secondary tumors are more aggressive compared with *Sfrp1*$^{-/-}$ primary tumors (Figure S2A). Moreover, we also performed limiting dilution assay where we transplanted 10,000, 5,000, and 1,000 CSCs from both the WT SCCs and *Sfrp1*$^{-/-}$ SCCs into the NOD/SCID mice. The results showed that mice transplanted with 10,000 *Sfrp1*$^{-/-}$ CSCs developed tumors within 4–5 weeks of transplantation, whereas mice with 10,000 WT CSCs developed tumors after 7–8 weeks (Figures 3D and 3E). Further, mice with 5,000 *Sfrp1*$^{-/-}$ CSCs developed tumors after 6–7 weeks and no tumors were observed in mice with 5,000 WT CSCs (Figure S2B). Moreover, no tumors were observed in mice transplanted with 1,000 CSCs from either WT or *Sfrp1*$^{-/-}$ SCCs (Figure S2C). The TPC frequency was calculated as reported earlier (Hu and Smyth, 2009), and we found that 1/8,442 (estimated value) *Sfrp1*$^{-/-}$ CSCs and 1/34,761 (estimated value) WT CSCs are able to form tumors when transplanted into NOD/SCID mice (Figure S2D). These results suggest that loss of *Sfrp1* results in aggressiveness of the CSCs with increased TPC frequency in *Sfrp1*$^{-/-}$ CSCs.

Expression Profiling on the CSCs of *Sfrp1* Knockouts Revealed Altered EMT Regulators and Growth Factor Signaling

To understand the changes in the expression of *Sfrp1* with time, we quantified *Sfrp1* mRNA levels in WT mouse epidermis at various time points, such as 5, 10, 15, and 20 weeks, during the DMBA/TPA treatment. The results showed a progressive decrease of *Sfrp1* with time in mouse epidermis with TPA treatment (Figure S3A). Further, the mRNA expression levels of *Sfrp1* were quantified in both the WT mouse normal epidermis and the chemically induced (DMBA/TPA) WT SCC, which showed a significant decrease in *Sfrp1* expression in WT SCC compared with WT normal epidermis (Figure S3B). Moreover, the mRNA quantification of *Sfrp1* in the WT CSC population versus the WT non-CSC population showed a significant decrease in *Sfrp1*

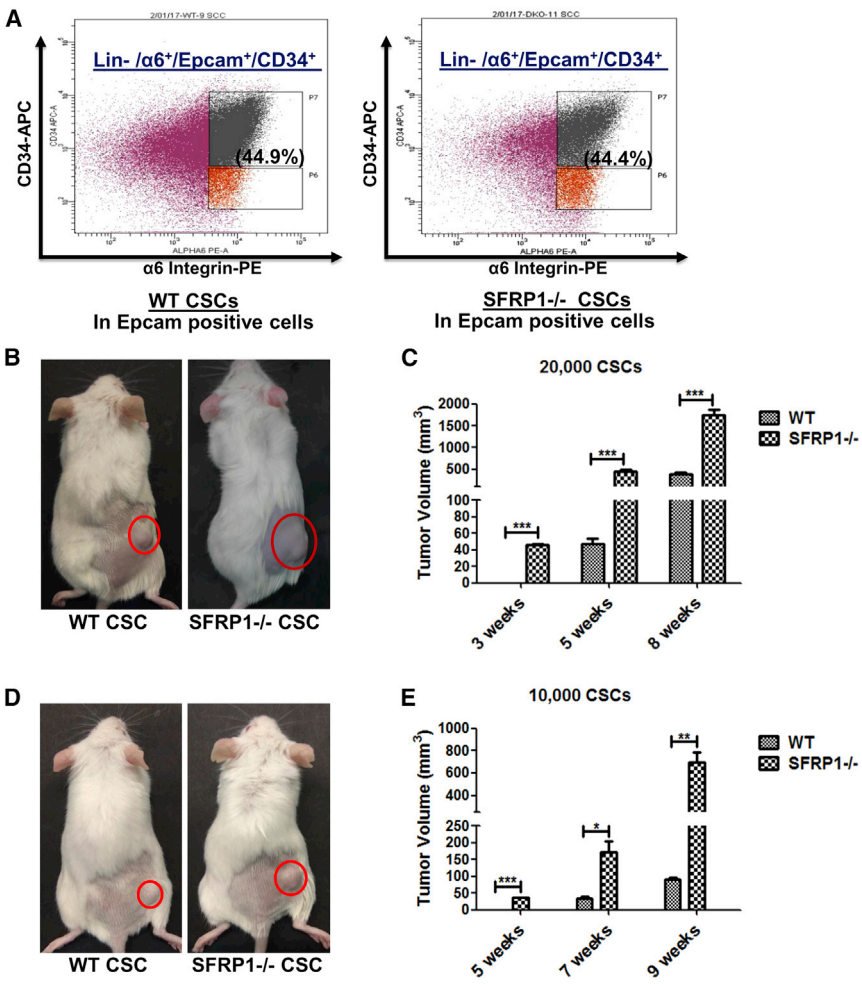

Figure 3. Increased Tumorigenic Potential in CSCs from *Sfrp1*$^{-/-}$ SCC

(A) FACS analysis of CSCs in both WT SCC and *Sfrp1*$^{-/-}$ SCC.

(B) *In vivo* tumorigenesis assay using 20,000 FACS-sorted CSCs from the WT SCC and *Sfrp1*$^{-/-}$ SCC transplanted into NOD/SCID mice. Tumor growth in NOD/SCID mice after 5 weeks of CSC transplantation is shown (n = 5 mice/genotype).

(C) Graphical representation of tumor volume at 3, 5, and 8 weeks in NOD/SCID mice after transplantation with 20,000 FACS-sorted CSCs from WT SCC and *Sfrp1*$^{-/-}$ SCC (n = 5 mice/genotype).

(D) *In vivo* tumorigenesis assay of 10,000 FACS-sorted CSCs from WT SCC and *Sfrp1*$^{-/-}$ SCC transplanted into NOD/SCID mice. Tumor growth in NOD/SCID mice after 7 weeks of CSC transplantation is shown (n = 5 mice/genotype).

(E) Graphical representation of tumor volume at 5, 7, and 9 weeks in NOD/SCID mice after transplantation with 10,000 FACS-sorted CSCs from WT SCC and *Sfrp1*$^{-/-}$ SCC (n = 5 mice/genotype).

WT, wild type; *Sfrp1*$^{-/-}$, homozygous knockout for *Sfrp1*; CSC, cancer stem cell; SCC, squamous cell carcinoma; FACS, fluorescence-activated cell sorting; Lin-, lineage negative (CD-31^{-ve}, CD-45^{-ve}, CD-140a^{-ve}), α6+, α6 positive. Data were analyzed by Student's t test and presented as means ± SEM. *p < 0.05, **p < 0.01, ***p < 0.001. See also Figure S2.

expression in WT CSCs compared with the WT non-CSC population (Figure S3C). Importantly, to investigate the molecular mechanism behind the increased tumorigenic potential of *Sfrp1*$^{-/-}$ CSCs, we performed expression profiling on WT and *Sfrp1*$^{-/-}$ CSCs (Figure 4A). The gene expression profile data showed that growth factor receptors (*Ghr*, *Pdgfra*, *Tgfbr3*, and *Eps8*) and their downstream signaling molecules (*Akt3* and *Mapk3/Erk1*), which are associated with tumor aggressiveness, metastatic potential, and proliferation, were highly upregulated in the *Sfrp1*$^{-/-}$ CSC population compared with WT CSCs (Figure 4B). Further, the genes involved in the cell to extracellular matrix interaction, such as *Spp1*, *Vcam1*, and *Fn1*, which are known to promote tumor invasion and metastasis, were highly upregulated in *Sfrp1*$^{-/-}$ CSCs. Moreover, EMT markers such as *Twist1*, *Twist2*, *Snail*, *Vimentin*, and *Zeb1* showed increased expression in the *Sfrp1*$^{-/-}$ CSCs, while E-cadherin (*Cdh1*), an epithelial marker, was highly downregulated (Figure 4B). The expression of the stem cell marker *Sox-2*, involved in regulating tumor initiation and CSC regulation, was upregulated by 4-fold. Further, expression of K8 (*K8*), a marker for highly invasive and undifferentiated skin tumor, was also higher by 4- to 5-fold. The gene expression profile data were further validated using quantitative real-time PCR, which was in congruence with the microarray data (Figures 4C–4G). This was further confirmed by performing IFA of K8, vimentin (VIM), and SOX-2 in both the *Sfrp1*$^{-/-}$ and the WT tumors, which showed higher expression of K8, VIM, and SOX-2 in the *Sfrp1*$^{-/-}$ tumors (Figures 5A–5F).

In addition, *Sfrp1*$^{-/-}$ CSCs showed a decrease in *Wnt3A* (canonical Wnt ligand) and increase in expression of *Wnt7B* (noncanonical Wnt ligand) (Figures S4A and S4B). SFRP1 was shown to bind and inhibit WNT7B (Rosso et al., 2005); therefore, loss of SFRP1 could enhance the WNT7B-mediated signaling cascade (WNT7B/JNK/c-JUN/c-FOS pathway) leading to the expression of *Sox-2*. Hence, we checked the expression of *c-Jun* and *c-Fos*, which showed upregulation in *Sfrp1*$^{-/-}$ CSCs compared with WT CSCs. Overall, the data suggest the loss of *Sfrp1* leads to accelerated tumor initiation with aggressiveness in

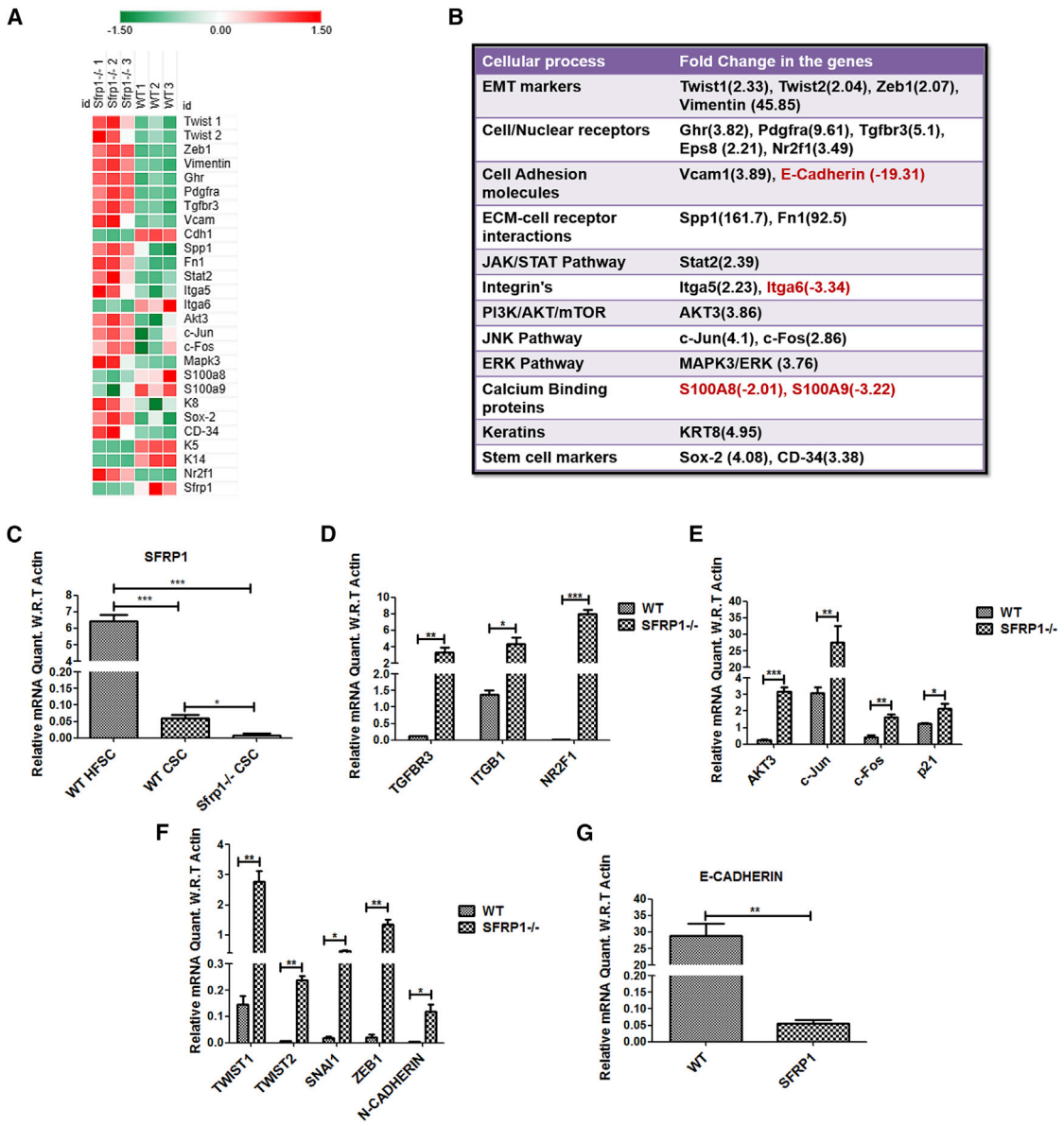

Figure 4. Altered Signaling in *Sfrp1*$^{-/-}$ CSCs Compared with WT CSCs

(A) Heatmap of the significantly deregulated genes between WT CSCs and *Sfrp1*$^{-/-}$ CSCs (n = 3 biological replicates/genotype).

(B) Expression profile of various pathways in *Sfrp1*$^{-/-}$ CSCs compared with WT CSCs.

(C) Graph representing the expression levels of the *Sfrp1* in WT HFSCs, WT CSCs, and *Sfrp1*$^{-/-}$ CSCs validated using quantitative real-time PCR (n = 3 biological replicates/genotype).

(D and E) Graphs representing the expression level changes in cell surface receptors and signaling molecules in WT CSCs and *Sfrp1*$^{-/-}$ CSCs validated using quantitative real-time PCR (n = 3 biological replicates/genotype).

(F and G) Graphs representing the expression level changes in EMT genes in WT CSCs and *Sfrp1*$^{-/-}$ CSCs validated using quantitative real-time PCR (n = 3 biological replicates/genotype).

FACS, fluorescence-activated cell sorting; HFSC, hair follicle stem cells; CSCs, cancer stem cells; EMT, epithelial to mesenchymal transition; WT, wild type; SFRP1$^{-/-}$, homozygous knockout for *Sfrp1*. The mRNA expression levels were normalized to the expression of β-actin. Data were analyzed by Student's t test and presented as means ± SEM. *p < 0.05, **p < 0.01, ***p < 0.001. See also Figures S3 and S4.

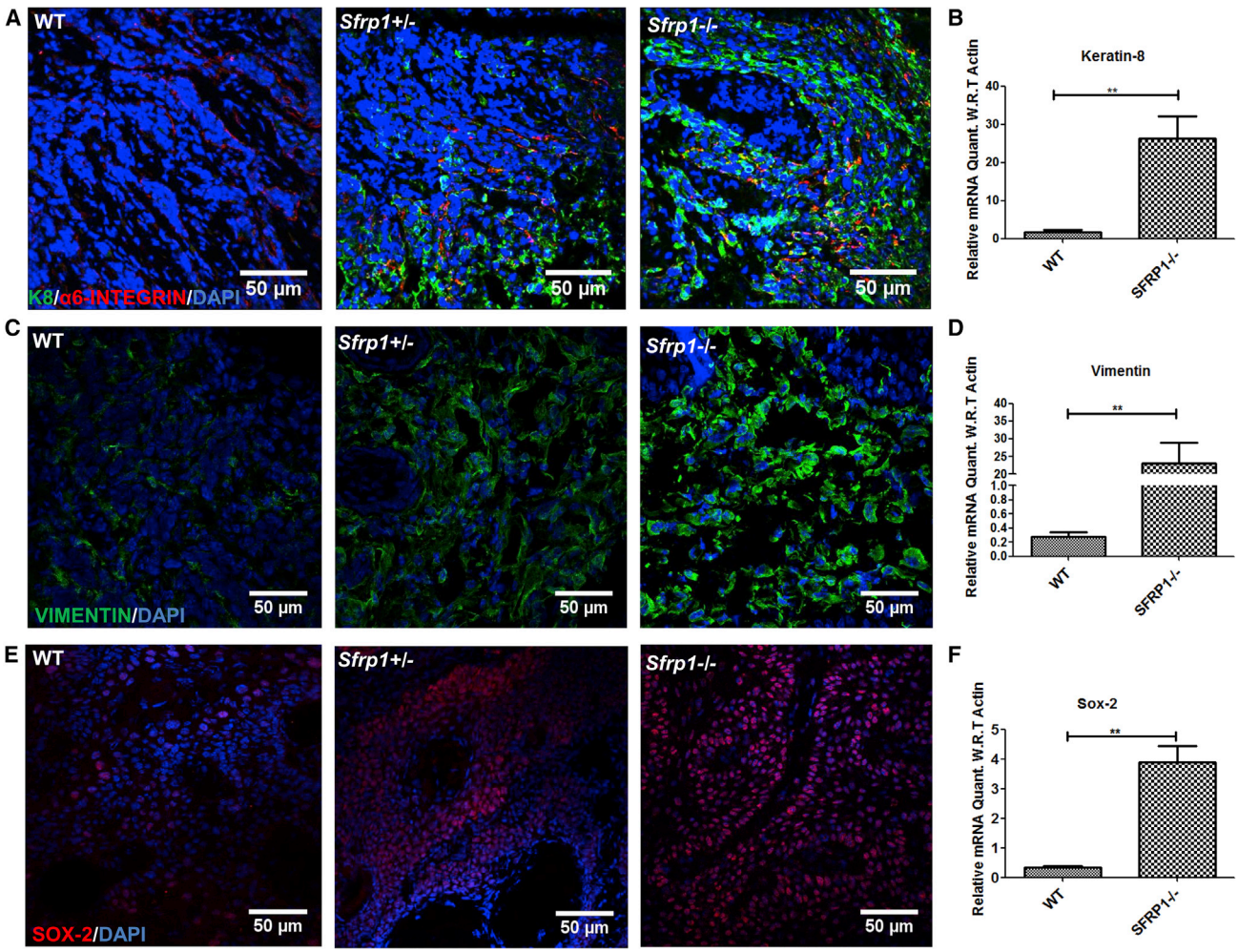

Figure 5. Enhanced Epithelial to Mesenchymal Transition and Stemness in *Sfrp1*$^{-/-}$ SCC

(A) IFA for keratin-8 (K8) and α6-integrin in WT SCC, *Sfrp1*$^{+/-}$ SCC, and *Sfrp1*$^{-/-}$ SCC (n = 5 biological replicates/genotype).

(B) Graphical representation of expression level changes in K8 of WT CSCs and *Sfrp1*$^{-/-}$ CSCs (n = 3 biological replicates/genotype).

(C) IFA for vimentin in WT SCC, *Sfrp1*$^{+/-}$ SCC, and *Sfrp1*$^{-/-}$ SCC (n = 5 biological replicates/genotype).

(D) Graphical representation of expression level changes in *Vimentin* in WT CSCs and *Sfrp1*$^{-/-}$ CSCs (n = 3 biological replicates/genotype).

(E) IFA for SOX-2 in WT SCC, *Sfrp1*$^{+/-}$ SCC, and *Sfrp1*$^{-/-}$ SCC (n = 5 biological replicates/genotype).

(F) Graphical representation of expression level changes in *Sox-2* in WT CSCs and *Sfrp1*$^{-/-}$ CSCs (n = 3biological replicates/genotype).

SCC, squamous cell carcinoma; CSCs, cancer stem cells; IFA, immunofluorescence assay; WT, wild type; *Sfrp1*$^{+/-}$, heterozygous for *Sfrp1*; *Sfrp1*$^{-/-}$, homozygous knockout for *Sfrp1*. Data were analyzed by Student's t test and presented as means ± SEM. Scale bar: 50 μm, $^{**}p < 0.01$.

CSCs by enhancing EMT signatures through altered signaling.

Loss of *SFRP1* Expression Leads to Upregulation of *SOX-2* in Human Skin SCC and HNSCC Tissues

Sfrp1$^{-/-}$ CSCs showed increased tumorigenic potential, and expression profiling revealed higher expression of the stem cell marker *Sox-2*. In order to determine whether the loss of *SFRP1* affects the stemness even in human skin cancers, we checked the expression levels of *SFRP1* and *SOX-2* in the human cutaneous SCC cell line A3886 and in the human keratinocyte cell line HaCaT. The results showed a decrease in the expression of *SFRP1* and increase in the expression of *SOX-2*, at both RNA and protein levels in A3886 compared with HaCaT. Moreover, treating A3886 cells with SFRP1-containing medium decreased the SOX-2 protein levels within these cells (Figures 6A and 6B). Further, as epidermis and oral epithelium share several

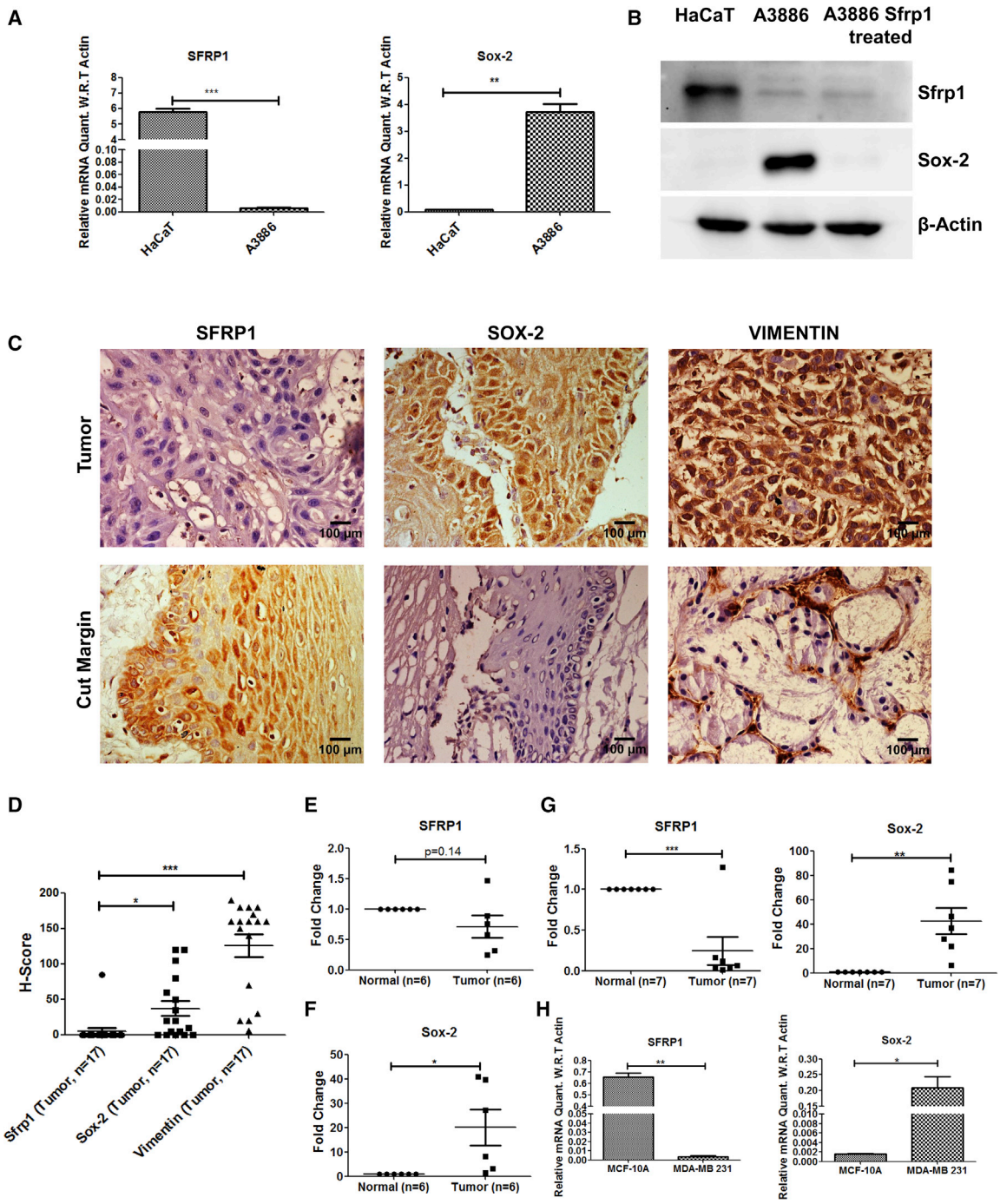

Figure 6. *SFRP1* Loss Showed Elevated *SOX-2* Expression in Skin Cancer, HNSCC, and Breast Cancer

(A) Graphical representation of *SFRP1* and *SOX-2* expression levels in A3886 (human cutaneous squamous cell carcinoma) cell line compared with HaCaT (human keratinocyte cell line) (n = 3 independent replicates).

(B) Western blot for SFRP1 and SOX-2 in HaCaT, A3886, and A3886 treated with SFRP1-containing medium for 48 h (n = 3 independent replicates).

(C) IHC for SFRP1, SOX-2, and VIM in HNSCC (buccal mucosa) samples and their adjacent cut margins (n = 3 independent replicates).

(D) Graph representing H score for SFRP1, SOX-2, and VIM within the tumor samples.

(E and F) Graphical representations of *SFRP1* and *SOX-2* expression levels in human HNSCC (buccal mucosa) samples compared with normal buccal mucosa (n = 6 for tumor and control samples).

(legend continued on next page)

structural and functional similarities, we sought to understand if a similar relation exists between *SFRP1* and *SOX-2* even in the HNSCC tissues. Hence, we performed a validation in human HNSCC (buccal mucosa) samples by doing immunohistochemistry (IHC) using the SOX-2, SFRP1, and VIM markers. We observed that the protein levels of SFRP1 were lower in tumor samples compared with the adjacent cut margins. Further, the expression of SOX-2 and VIM was higher in OSCC tumor sections compared with the adjacent cut margins (Figures 6C, 6D, and S5). These results were also further validated at the expression level in tumor samples of HNSCC (buccal mucosa) compared with their normal counterparts. The results showed a decrease in median expression of *SFRP1* and increase in *SOX-2* median expression in HNSCC (buccal mucosa) (Figures 6E and 6F). In order to further validate the inverse relation between *SFRP1* and *SOX-2* in a large cohort of tumor samples, we performed *in silico* analysis on HNSCC and SKCM (skin cutaneous melanoma) samples from the TCGA database. *SFRP1* expression is significantly decreased in HNSCC tumor samples (n = 521), compared with the normal controls (n = 43) (Figure S6A). The observed decrease is also stage dependent (n = 27, 71, 81, and 267 in stage I, stage II, stage III, and stage IV, respectively) (Figure S6B). Moreover, to determine if *SFRP1* and *SOX-2* are inversely related within HNSCC and SKCM, we first analyzed their expression in TCGA provisional data in HNSCC (n = 521) and in SKCM (n = 480). Further, *Z* scores were calculated for *SFRP1* and *SOX-2* tumor samples from normalized log2 transformed counts (Experimental Procedures). *SFRP1 Z* scores were sorted from low to high expression and the expression of *SOX-2* was determined in these samples (Figures S6C and S7A). Log odds ratio of −1.9 suggests a negative correlation between *SFRP1* and *SOX-2* in HNSCC. However, in SKCM, although we found a log odds ratio of 0.05, the trend of *SFRP1* and *SOX-2* inverse correlation was observed. Kaplan-Meier analysis of TCGA data of HNSCC and SKCM patients showed poor overall survival in the patients having low expression of *SFRP1* in HNSCC (n = 390) and SKCM (n = 345) compared with patients having high expression of *SFRP1* in HNSCC (n = 129) and SKCM (n = 114), with p values of 0.023 and 0.001, respectively (Figures S6D and S7D). All these data suggest an inverse correlation of *SFRP1* and *SOX-2* in HNSCC and SKCM samples.

Inverse Correlation of *SFRP1* and *SOX-2* Expression in Breast Cancer and Pancreatic Adenocarcinoma

In order to further validate the inverse correlation between *SFRP1* and *SOX-2* in other epithelial cancers, we checked the expression levels in breast cancer samples (Indian origin) along with their respective controls. The data showed a significant inverse correlation between *SFRP1* and *SOX-2* even in breast tumor samples (Figure 6G). Further, the levels of *SFRP1* and *SOX-2* were also assessed in breast cancer cell lines such as MDA-MB-231 (TNBC cell line) and control MCF-10A. The expression levels of *SFRP1* were highly reduced, whereas *SOX-2* was increased in MDA-MB-231 compared with MCF10A (Figure 6H). Further, we also analyzed *SFRP1* and *SOX-2* expression in TCGA provisional data in breast invasive carcinoma (n = 1105), and *Z* scores were calculated. *SFRP1* and *SOX-2* showed a negative correlation with a log odds ratio of −0.737 (Figure S7B). In addition, we also checked the *SFRP1* expression in pancreatic adenocarcinoma (PAAD) (n = 186). *Z* scores were calculated in PAAD, and we found a negative correlation with a log odds ratio of −3. Altogether, these data demonstrate an inverse correlation between *SFRP1* and *SOX-2* expression in breast and pancreatic cancer samples (Figures S7B and S7C). Further, Kaplan-Meier analysis of TCGA data of breast invasive carcinoma and PAAD patients showed poor overall survival in the patients with low expression of *SFRP1* in breast cancer (n = 808) and PAAD cancer (n = 132) compared with patients with high expression of *SFRP1* in breast (n = 273) and PAAD (n = 45), with p values of 0.011 and 0.025, respectively (Figures S7E and S7F). Overall, these data suggest an inverse correlation between *SFRP1* and *SOX-2* in breast cancer and PAAD.

DISCUSSION

SFRP1 is downregulated in various cancers, including skin, OSCC, breast cancers, etc. (Liang et al., 2015; Sogabe et al., 2008; Veeck et al., 2006). However, its role in tumor initiation and CSC regulation is yet to be discovered. Here, we attempted to unravel the role of *Sfrp1* in skin tumor initiation and CSC regulation. We have shown that *Sfrp1*$^{-/-}$ mice show increased sensitivity to chemical-induced carcinogenesis with an early tumor initiation. The tumor

(G) Graphical representation of *SFRP1* and *SOX-2* expression levels in breast tumor samples compared with normal breast tissue (n = 7 for tumor and control samples).

(H) Graphical representation of *SFRP1* and *SOX-2* expression levels in MDA-MB-231 cell line compared with MCF-10A (n = 3 independent replicates).

HNSCC, head and neck squamous cell carcinoma; EMT, epithelial to mesenchymal transition; IHC, immunohistochemistry. Data were analyzed by Student's t test and presented as means ± SEM. Scale bar: 50 μm, *p < 0.05, **p < 0.01, ***p < 0.001. See also Figures S5–S7.

characterization of *Sfrp1*$^{-/-}$ SCCs predominantly showed SCCs with a mixed phenotype and a few SCCs with a mesenchymal phenotype. However, the WT SCCs mostly showed a well-differentiated epithelial phenotype, with a few SCCs with a mixed phenotype. This result is in congruence with an earlier report, where tumors arising from HFSCs showed mostly a mixed phenotype and a few tumors with a mesenchymal phenotype, while tumors arising from IFE (interfollicular epidermis) stem cells showed a well-differentiated tumor phenotype (Latil et al., 2017). This indicates a possibility that the tumors of *Sfrp1*$^{-/-}$ mice may arise primarily from HFSCs as most of the *Sfrp1*$^{-/-}$ tumors are of mixed phenotype and a few *Sfrp1*$^{-/-}$ tumors have a mesenchymal phenotype. However, WT mouse tumors may mostly arise from IFE stem cells rather than HFSCs, as most of the tumors showed a well-differentiated epithelial phenotype. Moreover, high expression of *Sfrp1* in WT HFSCs might also prevent tumor formation from HFSCs within these mice.

Further, K8 expression is important for the tumor progression and EMT of SCC (Caulin et al., 1993). In the present study, *Sfrp1*$^{-/-}$ CSCs showed higher K8 expression compared with WT CSCs. Hence, *Sfrp1* may regulate the expression of K8 in the rapid progression of SCC, thereby leading to higher tumorigenic potential. Further, to explore whether the loss of *Sfrp1* has any effect on CSC regulation, we checked the CSC percentage in the WT SCCs and *Sfrp1*$^{-/-}$ SCCs, which showed no alteration in the percentage of CSCs; however, the *in vivo* tumorigenesis assay showed increased tumorigenic potential of the *Sfrp1*$^{-/-}$ CSCs compared with control. In addition, limiting dilution assay using 10,000, 5,000, and 1,000 CSCs from WT SCCs and *Sfrp1*$^{-/-}$ SCCs showed that *Sfrp1*$^{-/-}$ CSCs were able to form tumors in NOD/SCID mice at cell numbers as low as 10,000 and 5,000 CSCs with an estimated TPC efficiency of 1/8,442. However, WT CSCs were able to form tumors only from 10,000 CSCs and were unable to form tumors from 5,000 CSCs in NOD/SCID mice, raising the estimated TPC efficiency to 1/34,761. Moreover, no tumors were observed with 1,000 CSCs of both the WT and the *Sfrp1*$^{-/-}$ SCCs. This suggests that *Sfrp1* loss alters the expression of different genes that are required to regulate the tumorigenicity of CSCs. Further, we performed the gene expression profile on the CSCs of *Sfrp1*$^{-/-}$ SCC compared with control. Our data showed an increased expression of the genes involved in proliferation, such as *Akt3*. Overexpression of *Akt3/Mtor* is involved in the proliferation of prostate cancer cells and endows the CSC phenotype (Chang et al., 2013). Further, *Akt3* also regulates *p21* expression in prostate cancer cells, which is involved in cell proliferation and antiapoptotic activity (Lu et al., 2006). We have also observed an increase in the p21 expression levels in *Sfrp1*$^{-/-}$ CSCs, which is in congruence with our *in vivo* tumorigenic data. In addition, *Mapk3/Erk1* is overexpressed in *Sfrp1*$^{-/-}$ CSCs compared with WT CSCs. Activation of *ERK1/ERK2* in non-small cell lung cancer (Vicent et al., 2004) and breast cancer (Adeyinka et al., 2002) is associated with tumor advancement and aggressiveness. Therefore, the increased expression of *Erk1* may lead to the higher tumorigenic potential of *Sfrp1*$^{-/-}$ CSCs.

In addition, we have observed an increase in the expression of the *Wnt7B* (noncanonical Wnt ligand) in the *Sfrp1*$^{-/-}$ CSCs. It was previously reported that SFRP1 binds and inhibits WNT7B; therefore, knockout of SFRP1 would enhance the WNT7B-mediated noncanonical signaling pathway. Moreover, WNT7B activates JNK, which in turn activates c-JUN (Rosso et al., 2005). Further, c-JUN binds to the promoter region of *Sox-2*, thereby increasing *Sox-2* expression, which is involved in cancer stemness and aggressiveness (Boumahdi et al., 2014; Chang et al., 2013). Therefore, we have checked the expression levels of *c-Jun* and *Sox-2 in Sfrp1*$^{-/-}$ CSCs, which showed an increase in *c-Jun* and *Sox-2* expression. Hence, SOX-2 could be involved in the earlier tumor initiation and aggressiveness observed in *Sfrp1*$^{-/-}$ CSCs compared with WT CSCs.

Taking these results together, we propose a putative model at the molecular level that, in the absence of *Sfrp1*, WNT7B binds to its receptor and flux through the noncanonical pathway increases, which activates JNK downstream through dishevelled. The activated JNK further activates c-JUN, which then enters into the nucleus, where it binds and increases the expression of *Sox-2*. Hence, this increased expression of SOX-2 is responsible for increased tumorigenicity and aggressiveness through regulation of EMT markers. However, in-depth understanding of the molecular signaling mechanism should be investigated further.

Importantly, the data obtained from the murine skin model, i.e., the inverse correlation between *Sfrp1* and *Sox-2*, was extrapolated to human skin cancer, as *SFRP1* was shown to be lost due to promoter hypermethylation in human cutaneous SCC (Liang et al., 2015). The expression levels of *SOX-2* were higher and *SFRP1* levels were lower in the A3886 cell line compared with HaCaT. Further, treatment of A3886 cells with SFRP1 externally led to a decrease in the SOX-2 levels, establishing an inverse correlation between *SFRP1* and *SOX-2*. In addition, as epidermis shares certain similarities with oral and breast epithelia in tissue architecture and in tumor progression, we further expanded our studies to these tissues. Moreover, *SFRP1* is also lost in OSCC and in breast cancer due to promoter hypermethylation (Sogabe et al., 2008; Veeck et al., 2006). Hence, we sought to understand whether a similar kind of relation of *SFRP1* and *SOX-2* exists even in OSCC samples of Indian origin. We have observed that SFRP1 levels were lower in OSCC samples compared with the adjacent cut margins.

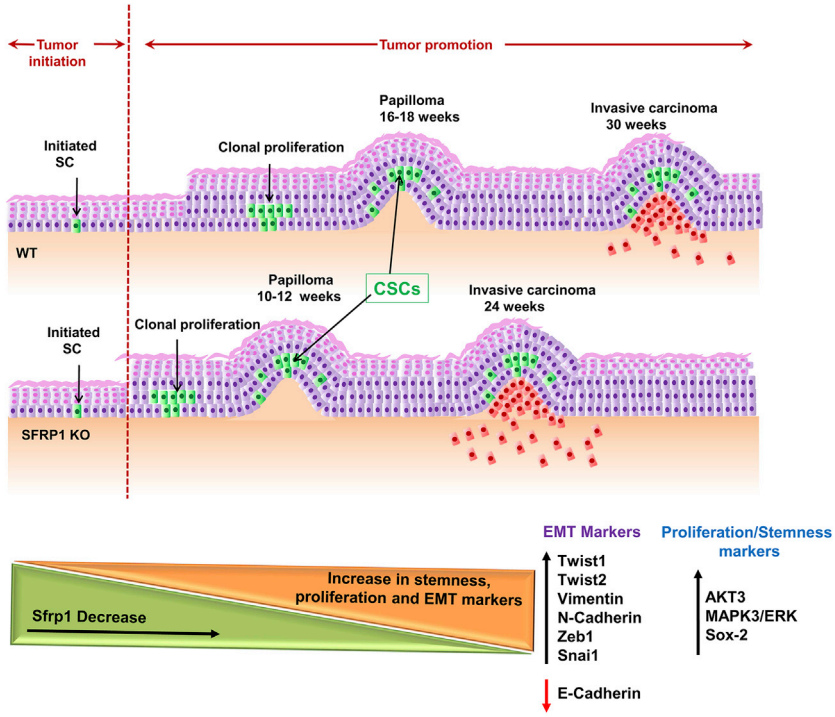

Figure 7. Schematic Representation of Accelerated Skin Tumor Initiation and CSC Regulation Due to Loss of *Sfrp1*

Schematic diagram illustrating time points of papilloma and SCC formation in WT and *Sfrp1*$^{-/-}$ mouse skin upon DMBA and TPA treatment. Induced skin carcinogenesis showed early tumor formation in *Sfrp1*$^{-/-}$ mice compared with WT mice. As *Sfrp1* decreases there is an increase in stemness (*Sox-2*), proliferation, and EMT markers in *Sfrp1*$^{-/-}$ CSCs.

WT, wild type; *Sfrp1*$^{-/-}$, homozygous knockout for *Sfrp1*; CSC, cancer stem cells; SCC, squamous cell carcinoma; DMBA, 7,12-dimethylbenz[a]anthracene; TPA, 12-O-tetradecanoyl phorbol-13-acetate; EMT, epithelial to mesenchymal transition.

Further, the expression of SOX-2 and VIM was higher in tumor sections compared with the adjacent cut margins, establishing an inverse correlation of *SFRP1* and *SOX-2* in OSCC samples. In addition we found a similar correlation in both breast tumor tissues and a breast cancer cell line (MDA-MB-231). In order to verify the observed correlation in a large cohort of samples, we used the TCGA database, where we found the inverse correlation in multiple epithelial cancers, such as SKCM, HNSCC, breast cancer, and PAAD.

In summary, we have shown that *Sfrp1* loss results in early tumor initiation and CSC regulation (Figure 7). Importantly, the knowledge obtained from the *in vivo* mouse skin carcinogenesis model was validated in multiple human epithelial cancers that showed that *Sfrp1* downregulation is associated with poor survival. This study provides compelling evidence for using murine epithelial models to uncover molecular signaling in human epithelial cancers. Overall, future studies are warranted in understanding the in-depth molecular mechanism of *Sfrp1* that is involved in CSC regulation with respect to tumor aggressiveness, proliferation, and EMT regulation, which may pave the way in the development of strategies for cancer.

EXPERIMENTAL PROCEDURES

Mice

Sfrp1 homozygous knockout (*Sfrp1*$^{-/-}$) mice were a gift from Dr. Akihiko Shimono, Japan. The animal study was approved by the ACTREC's Institutional Animal Ethics Committee. For the experiments, mice of all three genotypes, WT, *Sfrp1*$^{+/-}$ (heterozygous knockout), and *Sfrp1*$^{-/-}$ (homozygous knockout), were obtained by intercrossing *Sfrp1*$^{+/-}$ mice. The genotyping of these mice was performed as described previously (Satoh et al., 2006).

DMBA/TPA Treatments

We used the two-step chemically induced skin carcinogenesis protocol as described previously (Beck et al., 2015). Mice were topically treated with DMBA (mutagen) and TPA (promoting agent) for skin tumor generation. For complete details, please refer to the Supplemental Information.

Tumor Collection and Digestion for a Single-Cell Suspension

Tumors were dissected from mouse skin, and they were cleaned of any traces of normal skin, blood vessels, and connective tissue attached to them. For complete details please refer to the Supplemental Information.

Isolation of CSCs from SCC

After preparation of a single-cell suspension, the cells were stained using well-defined CSC markers, Lin$^-$/Epcam$^+$/α6 integrin$^+$/CD34$^+$, and CSCs were FACS sorted using FACSAria (BD Biosciences, San Jose, CA). For complete details please refer to the Supplemental Information.

Expression Profiling

FACS-sorted CSCs were utilized for the extraction of RNA. After the RNA quality was assessed, cDNA was prepared and expression

profiling was performed using a GeneChip MTA 1.0 array (Affymetrix, USA). For a detailed description of expression profiling and real-time PCR, please refer to the Supplemental Information.

Cell Lines and Tumor Tissue Samples

We have used A3886 (skin cutaneous SCC cell line, a generous gift from Dr. Colin Jamora's lab, Instem, Bangalore), MCF-10A (control), and MDA-MB-231 (TNBC) cell lines. These cell lines were cultured using DMEM containing 10% fetal bovine serum and 1% antibiotics (Invitrogen). The cell lines were passaged using 0.25% trypsin:EDTA solution and maintained at 37°C and 5% CO_2. The OSCC (advanced stage treatment naive samples) and breast tumor (invasive ductal carcinoma samples) tissue samples used in the study were approved by the Institutional Ethics Committee under project nos. 188 and 164, respectively.

H&E and Immunostaining on Tumor Sections

Tumor tissues were processed for preparation of paraffin blocks or directly embedded in the OCT compound and stored at −80°C. Subsequently, tumor histology was analyzed by H&E staining on the paraffin tissue sections. IFAs were performed as described previously (Waghmare et al., 2008). For detailed description of IFA and IHC, please refer to the Supplemental Information.

In Silico Analysis

The TCGA PANCAN normalized raw counts were obtained from the UCSC cancer genome browser to determine the expression level changes of *SFRP1* and *SOX-2* in normal versus tumor samples of HNSCC. The raw data for SKCM, breast, and PAAD cancers were obtained from cBioPortal. The *Z* scores were calculated and heatmap was constructed using R 3.3.3. For complete details please refer to the Supplemental Information.

In Vivo Tumorigenesis Assay

FACS-sorted CSCs were directly collected in 100 μL of E-Media, mixed with 50 μL of Matrigel, and injected into NOD/SCID mice subcutaneously. Tumor progression was recorded twice a week by taking photographs from the time of transplantation to the experimental endpoint. Tumor size was measured with a Vernier caliper every week from 2 to 15 weeks.

Statistical Analysis

Statistical analysis was performed for tumor incidences, tumor volume, real-time PCR, and FACS analysis by using unpaired two-tailed Student's t test with GraphPad Prism 5. Error bar indicates the mean ± SEM of the mean values: *$p < 0.05$, **$p < 0.01$, ***$p < 0.001$. The t.test function in R 3.3.3 was used to calculate the p value for TCGA data. The overall survival plots were plotted using Kaplan-Meier analysis. The p values for the survival data were determined using chi-squared analysis.

ACCESSION NUMBERS

The expression profile data have been submitted to the GEO database with accession no. GEO: GSE141176.

SUPPLEMENTAL INFORMATION

Supplemental Information can be found online at https://doi.org/10.1016/j.stemcr.2019.12.006.

AUTHOR CONTRIBUTIONS

S.K.W. conceived and designed the project and analyzed and interpreted the data; R.R.S. performed the experiments and analysis; R.M.S. and R.R.S. performed DMBA/TPA experiments and RNA extraction and analysis; P.S. performed the histology and helped with the animal work; S.S. performed the *in silico* data analysis and real-time PCR on HNSCC and breast samples; S.K.W. and R.R.S. performed RNA extraction for microarray and analyzed all the data; S.G. designed, analyzed, and wrote the *in silico* and *in vivo* validation data; P.C. provided the HNSCC tissue samples; P.G. performed IHC data analysis; S.K.W. analyzed all the data; and S.K.W. and R.R.S. wrote the manuscript.

ACKNOWLEDGMENTS

We thank Dr. Akihiko Shimono, Japan, for providing the *Sfrp1* knockout mice. We thank Ms. Sayoni Roy for discussion. We thank Colin Jamora, Instem, Bangalore, for providing the A3886 human SCC cell line. We thank the ACTREC animal house, flow cytometry, and microscopy facilities. R.R.S. and S.S. are supported by an ACTREC fellowship. This work was supported by Department of Biotechnology (DBT), India.

Received: August 18, 2018
Revised: December 5, 2019
Accepted: December 9, 2019
Published: January 9, 2020

REFERENCES

Adeyinka, A., Nui, Y., Cherlet, T., Snell, L., Watson, P.H., and Murphy, L.C. (2002). Activated mitogen-activated protein kinase expression during human breast tumorigenesis and breast cancer progression. Clin. Cancer Res. *8*, 1747–1753.

Al-Hajj, M., Wicha, M.S., Benito-Hernandez, A., Morrison, S.J., and Clarke, M.F. (2003). Prospective identification of tumorigenic breast cancer cells. Proc. Natl. Acad. Sci. U S A *100*, 3983–3988.

Argiris, A. (2015). EGFR inhibition for recurrent or metastatic HNSCC. Lancet Oncol. *16*, 488–489.

Arihiro, K., Kaneko, M., Fujii, S., Inai, K., and Yokosaki, Y. (2000). Significance of alpha 9 beta 1 and alpha v beta 6 integrin expression in breast carcinoma. Breast Cancer *7*, 19–26.

Batlle, E., and Clevers, H. (2017). Cancer stem cells revisited. Nat. Med. *23*, 1124–1134.

Beck, B., Lapouge, G., Rorive, S., Drogat, B., Desaedelaere, K., Delafaille, S., Dubois, C., Salmon, I., Willekens, K., Marine, J.C., et al. (2015). Cell Stem Cell. Different levels of Twist1 regulate skin tumor initiation, stemness, and progression *16*, 67–79.

Bernemann, C., Hulsewig, C., Ruckert, C., Schafer, S., Blumel, L., Hempel, G., Gotte, M., Greve, B., Barth, P.J., Kiesel, L., et al. (2014). Influence of secreted frizzled receptor protein 1 (SFRP1)

on neoadjuvant chemotherapy in triple negative breast cancer does not rely on WNT signaling. Mol. Cancer *13*, 174.

Blanpain, C., Lowry, W.E., Pasolli, H.A., and Fuchs, E. (2006). Canonical notch signaling functions as a commitment switch in the epidermal lineage. Genes Dev. *20*, 3022–3035.

Bonnet, D., and Dick, J.E. (1997). Human acute myeloid leukemia is organized as a hierarchy that originates from a primitive hematopoietic cell. Nat. Med. *3*, 730–737.

Boumahdi, S., Driessens, G., Lapouge, G., Rorive, S., Nassar, D., Le Mercier, M., Delatte, B., Caauwe, A., Lenglez, S., Nkusi, E., et al. (2014). SOX2 controls tumour initiation and cancer stem-cell functions in squamous-cell carcinoma. Nature *511*, 246–250.

Caulin, C., Bauluz, C., Gandarillas, A., Cano, A., and Quintanilla, M. (1993). Changes in keratin expression during malignant progression of transformed mouse epidermal keratinocytes. Exp. Cell Res. *204*, 11–21.

Chang, L., Graham, P.H., Hao, J., Ni, J., Bucci, J., Cozzi, P.J., Kearsley, J.H., and Li, Y. (2013). Acquisition of epithelial-mesenchymal transition and cancer stem cell phenotypes is associated with activation of the PI3K/Akt/mTOR pathway in prostate cancer radioresistance. Cell Death Dis. *4*, e875.

Clevers, H. (2006). Wnt/beta-catenin signaling in development and disease. Cell *127*, 469–480.

Davaadorj, M., Imura, S., Saito, Y.U., Morine, Y., Ikemoto, T., Yamada, S., Takasu, C., Hiroki, T., Yoshikawa, M., and Shimada, M. (2016). Loss of SFRP1 expression is associated with poor prognosis in hepatocellular carcinoma. Anticancer Res. *36*, 659–664.

De Benedetto, A., Qualia, C.M., Baroody, F.M., and Beck, L.A. (2008). Filaggrin expression in oral, nasal, and esophageal mucosa. J. Invest. Dermatol. *128*, 1594–1597.

Faraldo, M.M., Teuliere, J., Deugnier, M.A., Taddei-De La Hosseraye, I., Thiery, J.P., and Glukhova, M.A. (2005). Myoepithelial cells in the control of mammary development and tumorigenesis: data from genetically modified mice. J. Mammary Gland Biol. Neoplasia *10*, 211–219.

Fillies, T., Werkmeister, R., Packeisen, J., Brandt, B., Morin, P., Weingart, D., Joos, U., and Buerger, H. (2006). Cytokeratin 8/18 expression indicates a poor prognosis in squamous cell carcinomas of the oral cavity. BMC Cancer *6*, 10.

Gu, B., Watanabe, K., Sun, P., Fallahi, M., and Dai, X. (2013). Chromatin effector Pygo2 mediates Wnt-notch crosstalk to suppress luminal/alveolar potential of mammary stem and basal cells. Cell Stem Cell *13*, 48–61.

Hu, Y., and Smyth, G.K. (2009). ELDA: extreme limiting dilution analysis for comparing depleted and enriched populations in stem cell and other assays. J. Immunol. Methods *347*, 70–78.

Huebner, R.J., Lechler, T., and Ewald, A.J. (2014). Developmental stratification of the mammary epithelium occurs through symmetry-breaking vertical divisions of apically positioned luminal cells. Development *141*, 1085–1094.

Karamboulas, C., and Ailles, L. (2013). Developmental signaling pathways in cancer stem cells of solid tumors. Biochim. Biophys. Acta *1830*, 2481–2495.

Kawano, Y., and Kypta, R. (2003). Secreted antagonists of the Wnt signalling pathway. J. Cell Sci. *116*, 2627–2634.

Larjava, H., Koivisto, L., Hakkinen, L., and Heino, J. (2011). Epithelial integrins with special reference to oral epithelia. J. Dental Res. *90*, 1367–1376.

Latil, M., Nassar, D., Beck, B., Boumahdi, S., Wang, L., Brisebarre, A., Dubois, C., Nkusi, E., Lenglez, S., Checinska, A., et al. (2017). Cell-type-specific chromatin states differentially prime squamous cell carcinoma tumor-initiating cells for epithelial to mesenchymal transition. Cell Stem Cell *20*, 191–204.e5.

Liang, J., Kang, X., Halifu, Y., Zeng, X., Jin, T., Zhang, M., Luo, D., Ding, Y., Zhou, Y., Yakeya, B., et al. (2015). Secreted frizzled-related protein promotors are hypermethylated in cutaneous squamous carcinoma compared with normal epidermis. BMC Cancer *15*, 641.

Liao, W.S., Ho, Y., Lin, Y.W., Naveen Raj, E., Liu, K.K., Chen, C., Zhou, X.Z., Lu, K.P., and Chao, J.I. (2019). Targeting EGFR of triple-negative breast cancer enhances the therapeutic efficacy of paclitaxel- and cetuximab-conjugated nanodiamond nanocomposite. Acta Biomater. *86*, 395–405.

Lien, W.H., Guo, X., Polak, L., Lawton, L.N., Young, R.A., Zheng, D., and Fuchs, E. (2011). Genome-wide maps of histone modifications unwind in vivo chromatin states of the hair follicle lineage. Cell Stem Cell *9*, 219–232.

Lim, X., and Nusse, R. (2013). Wnt signaling in skin development, homeostasis, and disease. Cold Spring Harb. Perspect. Biol. *5*, a008029.

Liu, F., and Millar, S.E. (2010). Wnt/beta-catenin signaling in oral tissue development and disease. J. Dental Res. *89*, 318–330.

Lu, S., Ren, C., Liu, Y., and Epner, D.E. (2006). PI3K-Akt signaling is involved in the regulation of p21(WAF/CIP) expression and androgen-independent growth in prostate cancer cells. Int. J. Oncol. *28*, 245–251.

Lu, X., Lu, D., Scully, M., and Kakkar, V. (2008). The role of integrins in cancer and the development of anti-integrin therapeutic agents for cancer therapy. Perspect. Med. Chem. *2*, 57–73.

Matsuyama, M., Aizawa, S., and Shimono, A. (2009). Sfrp controls apicobasal polarity and oriented cell division in developing gut epithelium. PLoS Genet. *5*, e1000427.

Meng, Y., Wang, Q.G., Wang, J.X., Zhu, S.T., Jiao, Y., Li, P., and Zhang, S.T. (2011). Epigenetic inactivation of the SFRP1 gene in esophageal squamous cell carcinoma. Dig. Dis. Sci. *56*, 3195–3203.

Morel, A.P., Lievre, M., Thomas, C., Hinkal, G., Ansieau, S., and Puisieux, A. (2008). Generation of breast cancer stem cells through epithelial-mesenchymal transition. PLoS One *3*, e2888.

Muroyama, A., and Lechler, T. (2012). Polarity and stratification of the epidermis. Semin. Cell Dev. Biol. *23*, 890–896.

Nassar, D., and Blanpain, C. (2016). Cancer stem cells: basic concepts and therapeutic implications. Annu. Rev. Pathol. *11*, 47–76.

Owens, D.M., Romero, M.R., Gardner, C., and Watt, F.M. (2003). Suprabasal alpha6beta4 integrin expression in epidermis results in enhanced tumourigenesis and disruption of TGFbeta signalling. J. Cell Sci. *116*, 3783–3791.

Porcheri, C., Meisel, C.T., and Mitsiadis, T. (2019). Multifactorial contribution of notch signaling in head and neck squamous cell carcinoma. Int. J. Mol. Sci. *20*, 1520.

Presland, R.B., and Dale, B.A. (2000). Epithelial structural proteins of the skin and oral cavity: function in health and disease. Crit. Rev. Oral Biol. Med. *11*, 383–408.

Prince, M.E., Sivanandan, R., Kaczorowski, A., Wolf, G.T., Kaplan, M.J., Dalerba, P., Weissman, I.L., Clarke, M.F., and Ailles, L.E. (2007). Identification of a subpopulation of cells with cancer stem cell properties in head and neck squamous cell carcinoma. Proc. Natl. Acad. Sci. U S A *104*, 973–978.

Ramos, D.M., But, M., Regezi, J., Schmidt, B.L., Atakilit, A., Dang, D., Ellis, D., Jordan, R., and Li, X. (2002). Expression of integrin beta 6 enhances invasive behavior in oral squamous cell carcinoma. Matrix Biol. *21*, 297–307.

Regan, J.L., Sourisseau, T., Soady, K., Kendrick, H., McCarthy, A., Tang, C., Brennan, K., Linardopoulos, S., White, D.E., and Smalley, M.J. (2013). Aurora A kinase regulates mammary epithelial cell fate by determining mitotic spindle orientation in a Notch-dependent manner. Cell Rep. *4*, 110–123.

Renstrom, J., Istvanffy, R., Gauthier, K., Shimono, A., Mages, J., Jardon-Alvarez, A., Kroger, M., Schiemann, M., Busch, D.H., Esposito, I., et al. (2009). Secreted frizzled-related protein 1 extrinsically regulates cycling activity and maintenance of hematopoietic stem cells. Cell Stem Cell *5*, 157–167.

Rosso, S.B., Sussman, D., Wynshaw-Boris, A., and Salinas, P.C. (2005). Wnt signaling through Dishevelled, Rac and JNK regulates dendritic development. Nat. Neurosci. *8*, 34–42.

Satoh, W., Gotoh, T., Tsunematsu, Y., Aizawa, S., and Shimono, A. (2006). Sfrp1 and Sfrp2 regulate anteroposterior axis elongation and somite segmentation during mouse embryogenesis. Development *133*, 989–999.

Sogabe, Y., Suzuki, H., Toyota, M., Ogi, K., Imai, T., Nojima, M., Sasaki, Y., Hiratsuka, H., and Tokino, T. (2008). Epigenetic inactivation of SFRP genes in oral squamous cell carcinoma. Int. J. Oncol. *32*, 1253–1261.

Song, X.L., Huang, B., Zhou, B.W., Wang, C., Liao, Z.W., Yu, Y., and Zhao, S.C. (2018). miR-1301-3p promotes prostate cancer stem cell expansion by targeting SFRP1 and GSK3beta. Biomed. Pharmacother. *99*, 369–374.

Steinhart, Z., and Angers, S. (2018). Wnt signaling in development and tissue homeostasis. Development *145*, dev146589.

Thiery, J.P., Acloque, H., Huang, R.Y., and Nieto, M.A. (2009). Epithelial-mesenchymal transitions in development and disease. Cell *139*, 871–890.

Tumbar, T., Guasch, G., Greco, V., Blanpain, C., Lowry, W.E., Rendl, M., and Fuchs, E. (2004). Defining the epithelial stem cell niche in skin. Science *303*, 359–363.

Uribe, P., and Gonzalez, S. (2011). Epidermal growth factor receptor (EGFR) and squamous cell carcinoma of the skin: molecular bases for EGFR-targeted therapy. Pathol. Res. Pract. *207*, 337–342.

Veeck, J., Niederacher, D., An, H., Klopocki, E., Wiesmann, F., Betz, B., Galm, O., Camara, O., Durst, M., Kristiansen, G., et al. (2006). Aberrant methylation of the Wnt antagonist SFRP1 in breast cancer is associated with unfavourable prognosis. Oncogene *25*, 3479–3488.

Vicent, S., Lopez-Picazo, J.M., Toledo, G., Lozano, M.D., Torre, W., Garcia-Corchon, C., Quero, C., Soria, J.C., Martin-Algarra, S., Manzano, R.G., et al. (2004). ERK1/2 is activated in non-small-cell lung cancer and associated with advanced tumours. Br. J. Cancer *90*, 1047–1052.

Waghmare, S.K., Bansal, R., Lee, J., Zhang, Y.V., McDermitt, D.J., and Tumbar, T. (2008). Quantitative proliferation dynamics and random chromosome segregation of hair follicle stem cells. EMBO J. *27*, 1309–1320.

Wellner, U., Schubert, J., Burk, U.C., Schmalhofer, O., Zhu, F., Sonntag, A., Waldvogel, B., Vannier, C., Darling, D., zur Hausen, A., et al. (2009). The EMT-activator ZEB1 promotes tumorigenicity by repressing stemness-inhibiting microRNAs. Nat. Cell Biol. *11*, 1487–1495.

Stem Cell Reports, Volume *14*

Supplemental Information

SFRP1 in Skin Tumor Initiation and Cancer Stem Cell Regulation with Potential Implications in Epithelial Cancers

Raghava R. Sunkara, Rahul M. Sarate, Priyanka Setia, Sanket Shah, Sanjay Gupta, Pankaj Chaturvedi, Poonam Gera, and Sanjeev K. Waghmare

Supplemental information

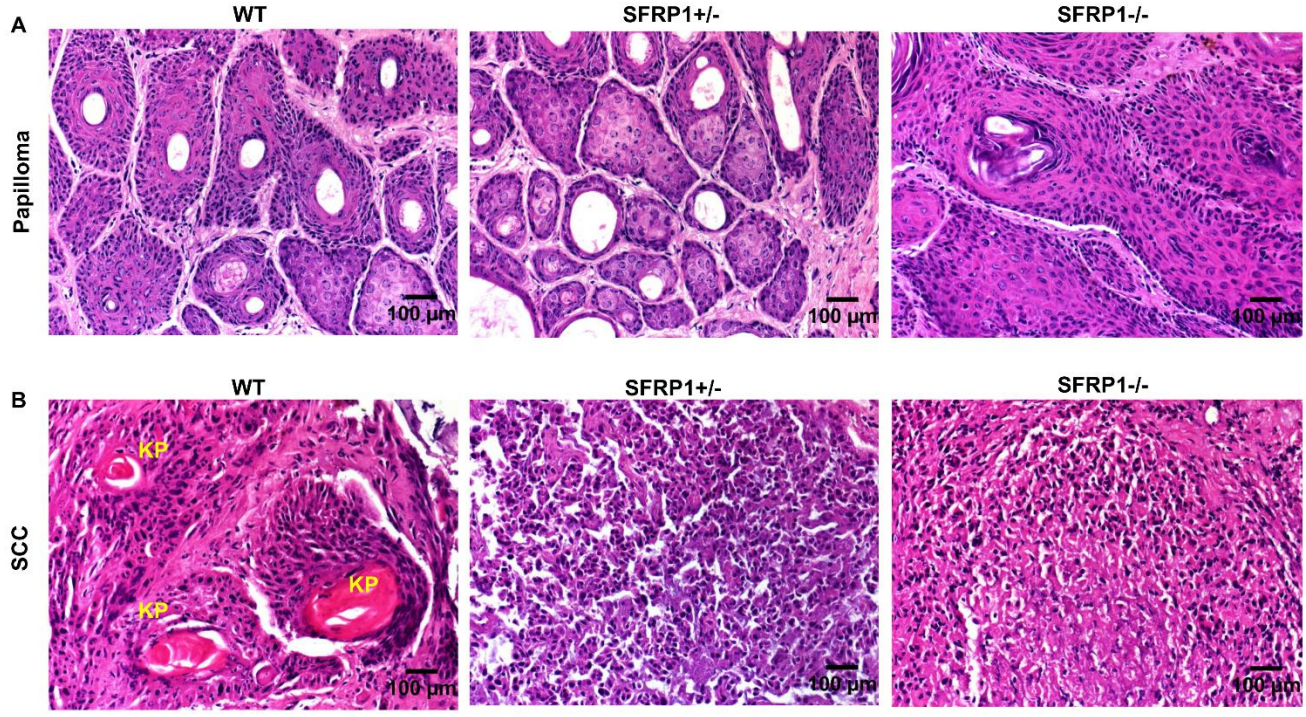

Figure S1: *Sfrp1* loss results in increased mesenchymal phenotype in SCC. Related to Figure 1.

Representative images of hematoxylin and eosin (H&E) stained 5µm thick paraffin embedded sections from **A**) Papilloma and **B**) Squamous cell carcinoma (SCC) of WT, *Sfrp1*$^{+/-}$ and *Sfrp1*$^{-/-}$ mice.

WT= Wild type, *Sfrp1*$^{+/-}$= heterozygous for *Sfrp1*, *Sfrp1*$^{-/-}$= homozygous knockout for *Sfrp1*, SCC= Squamous cell carcinoma, (n=6 mice/ genotype, KP= keratin pearl, scale bar: 100µm)

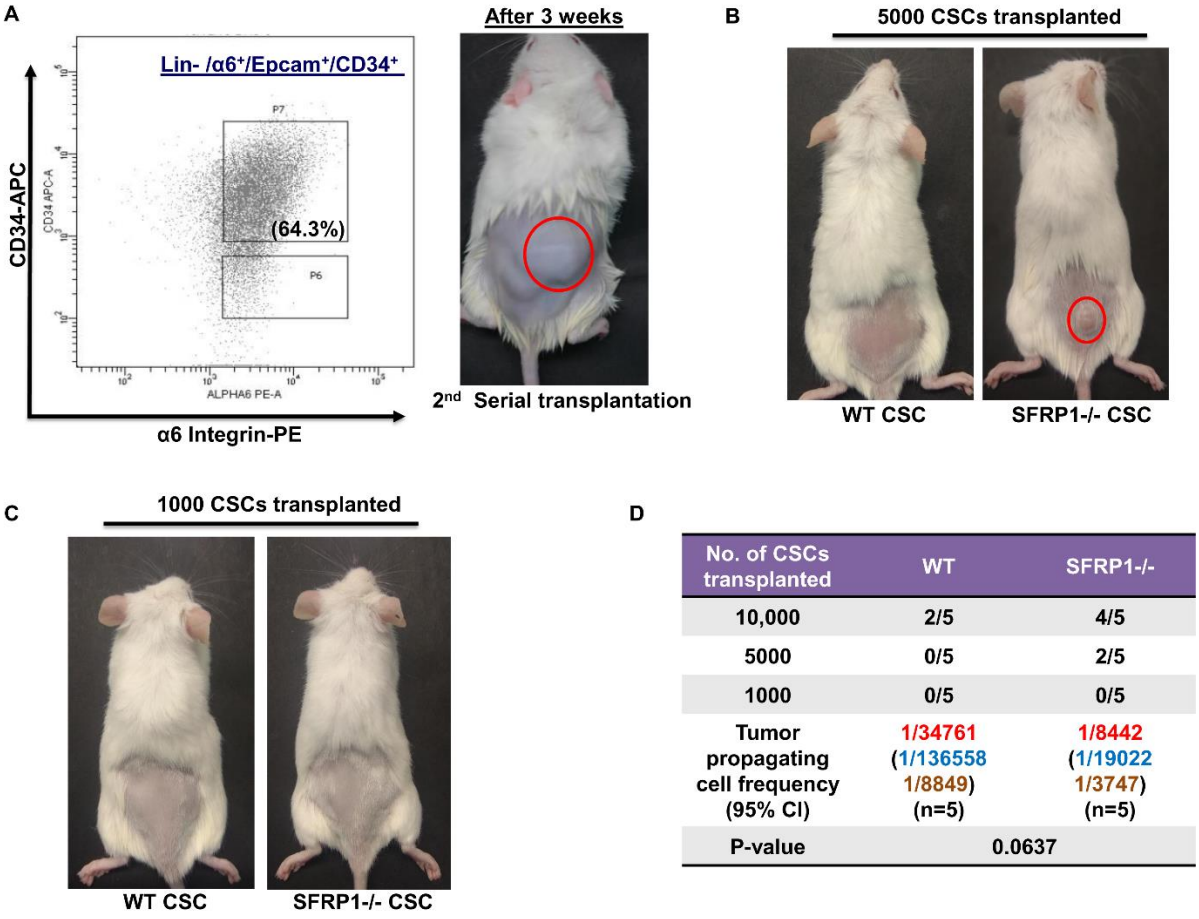

No. of CSCs transplanted	WT	SFRP1-/-
10,000	2/5	4/5
5000	0/5	2/5
1000	0/5	0/5
Tumor propagating cell frequency (95% CI)	1/34761 (1/136558 1/8849) (n=5)	1/8442 (1/19022 1/3747) (n=5)
P-value	0.0637	

Figure S2: Enhanced tumor propagating cell (TPC) frequency in *Sfrp1*$^{-/-}$ CSC. Related to Figure 3.

- **A.** FACS analysis to estimate the CSCs percentage in tertiary tumors. 20,000 FACS sorted *Sfrp1*$^{-/-}$ CSCs from secondary tumors were transplanted into NOD/SCID mice and tertiary tumor growth after 3weeks of transplantation.
- **B.** Limiting dilution assay using 5,000 FACS sorted CSCs from WT SCC and *Sfrp1*$^{-/-}$ SCC transplanted into NOD/SCID mice (n=5). Tumor growth in NOD/SCID mice after 9 weeks of CSC transplantation.
- **C.** Limiting dilution assay using 1000 FACS sorted CSCs from WT SCC and *Sfrp1*$^{-/-}$ SCC transplanted into NOD/SCID mice (n=5). No tumor growth in NOD/SCID mice was observed even after 14 weeks of CSC transplantation.
- **D.** Summary of TPC frequency estimated by the transplantation of limiting dilution of CSCs from WT SCC and *Sfrp1*$^{-/-}$ SCC into NOD/SCID mice. The data are represented in the ratio of transplantations that formed tumors out of total number of transplantations. The ratio in red color represent the estimated TPC frequency, while the ratios in blue and brown represent the lower and upper estimates of TPC respectively.

CSC= cancer stem cell, SCC= Squamous cell carcinoma, WT= Wild type, *Sfrp1*$^{-/-}$= homozygous knockout for *Sfrp1*, FACS= Fluorescent activated cell sorting, TPC= tumor propagating cell, n=5 mice/ genotype. TPC frequency was calculated by using ELDA (Extreme Limiting Dilution Analysis) software.

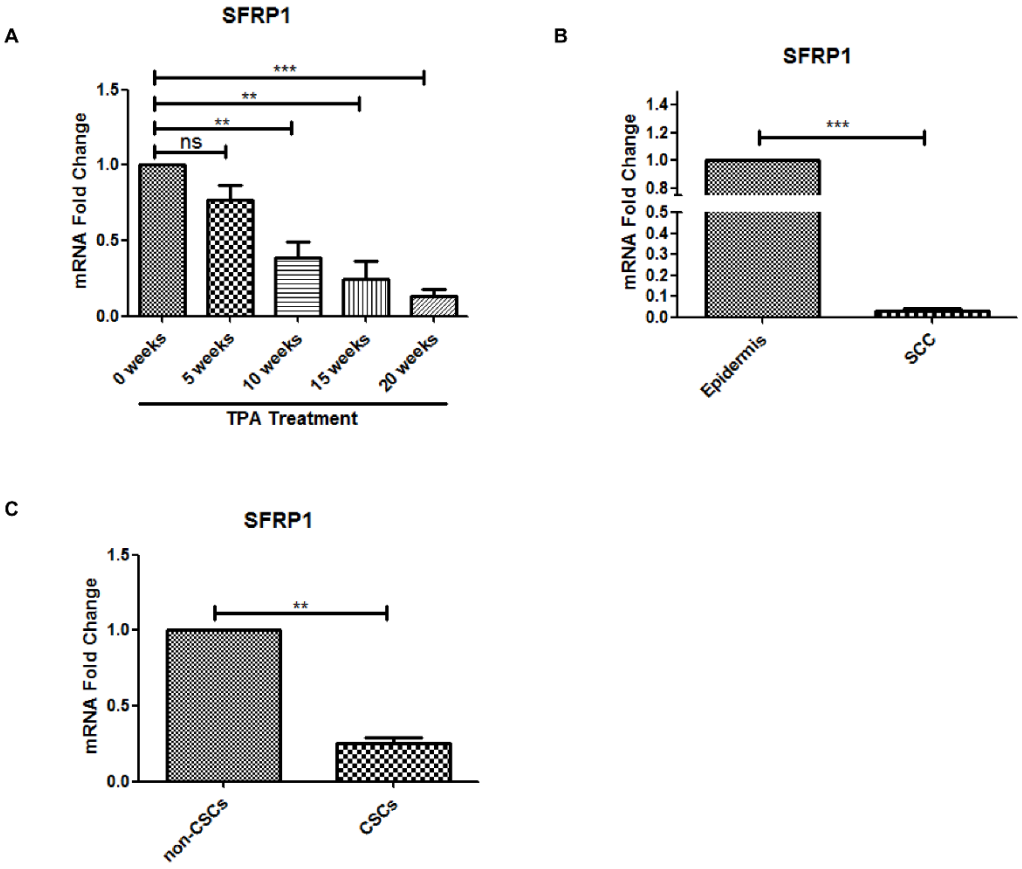

Figure S3: Expression level changes in *Sfrp1* at different time points during DMBA/TPA treatment. Related to Figure 4.

- **A)** Graphical representation of the mRNA expression levels of *Sfrp1* in WT mice epidermis at 5weeks, 10weeks, 15weeks and 20weeks during DMBA/TPA treatment
- **B)** Graphical representation of *Sfrp1*mRNA expression levels in WT epidermis as compared to WT SCC
- **C)** Graphical representation of *Sfrp1* mRNA expression levels in CSC Vs non-CSCs in WT SCC

CSC= cancer stem cell, Non-CSC= non Cancer Stem Cells, SCC= Squamous cell carcinoma, Data are presented as mean ± SEM and were analyzed by student's t-test. n=3 mice/ genotype (* = P<0.05, ** = p<0.01, ***=P<0.001)

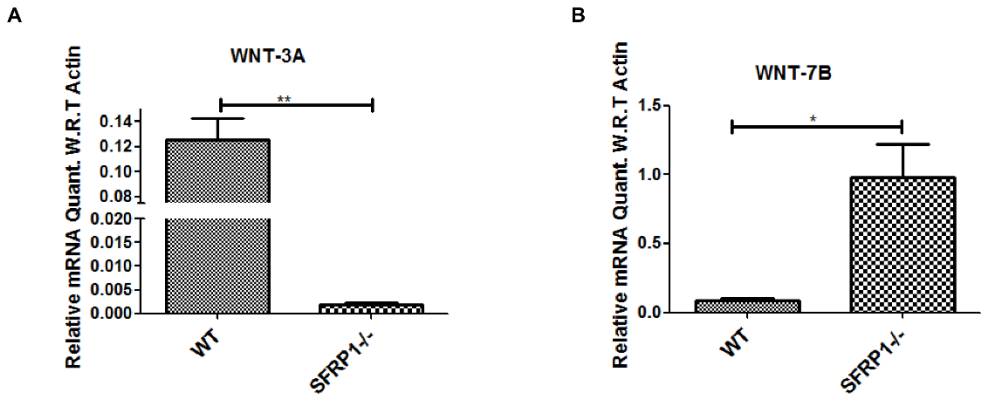

Figure S4: Altered expression of Wnt canonical and non-canonical ligands. Related to Figure 4.

A) Graphical representation of mRNA expression levels of Wnt-3A in WT and *Sfrp1*$^{-/-}$ CSCs

B) Graphical representation of mRNA expression levels of Wnt-7B in WT and *Sfrp1*$^{-/-}$ CSCs

WT= Wild type, *Sfrp1*$^{-/-}$= homozygous knockout for *Sfrp1*, SCC= Squamous cell carcinoma. The expression levels were normalized to the expression of β-Actin. Data are presented as mean ± SEM and were analyzed by student's t-test. n=3 mice/ genotype, scale bar= 50μm. (* = P<0.05, ** = p<0.01)

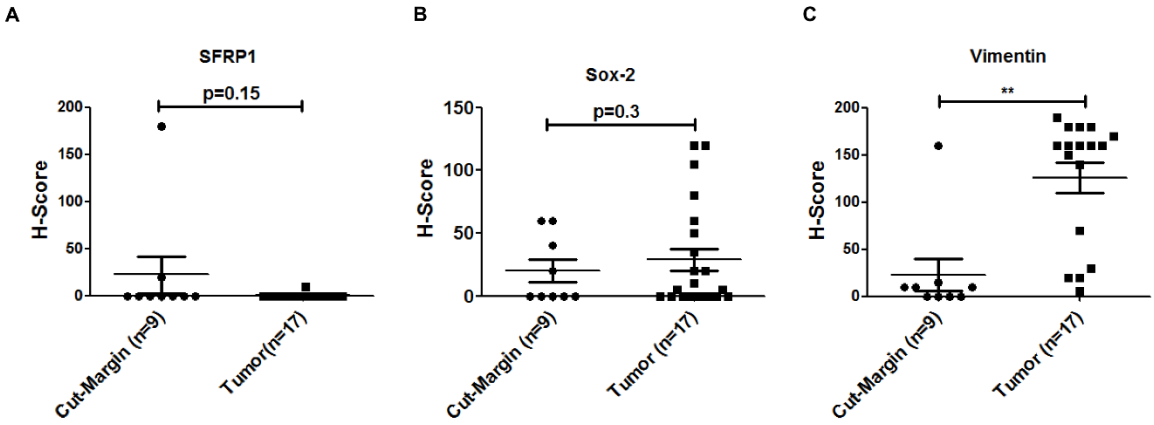

Figure S5: Comparative analysis of protein expression levels between OSCC tumors and adjacent cut margins. Related to Figure 6.

Immunohistochemistry (IHC) was performed for SFRP1, SOX-2, and VIMENTIN in both OSCC tumors and cut margins. The staining intensity was calculated and the H-scores were plotted for **A)** SFRP1 **B)** SOX-2 and **C)** VIMENTIN between tumor samples and their adjacent cut margins.

OSCC= Oral squamous cell carcinoma. Data are presented as mean ± SEM and were analyzed by student's t-test. (* = $P<0.05$, ** = $p<0.01$)

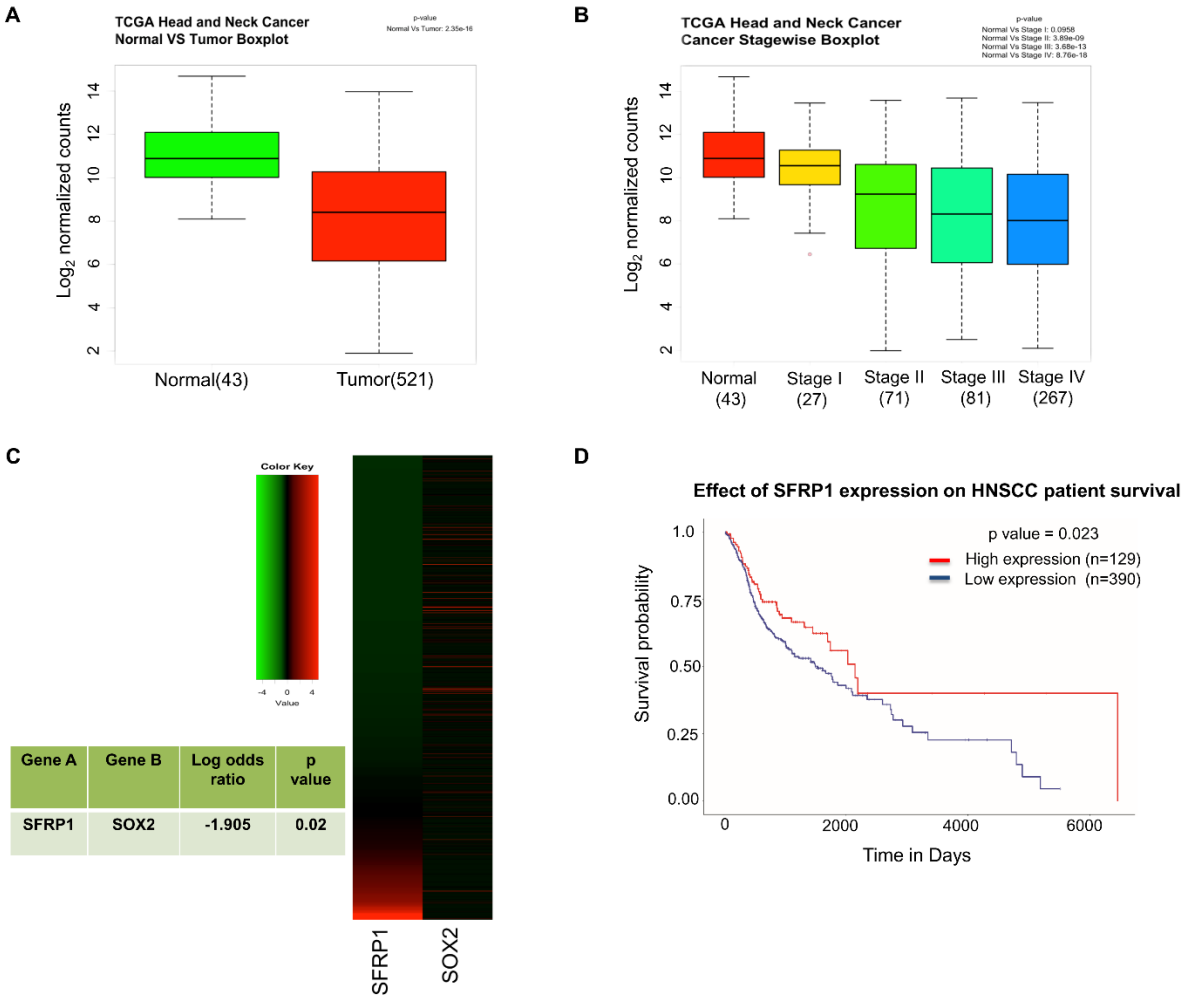

Figure S6: *SFRP1* expression was significantly low in HNSCC patients within TCGA data. Related to Figure 6.

A) *SFRP1* mRNA expression in non-tumor (normal) and tumor HNSCC samples respectively (n=43 for normal and n=521 for tumor)

B) *SFRP1* mRNA expression in normal, stage-I, stage-II, stage-III and stage-IV tumor samples respectively (normal: n=43, stage-I: n=27, stage-II: n=71, stage-III: n=81, stage-IV: n=267)

C) Heat map of *SFRP1* and *SOX2* expression in tumor samples showed inverse correlation. Patients were sorted from *SFRP1* low to high expression (Z< -1.5 is down-regulation and Z> 1.5 is up-regulation)

D) Survival analysis of TCGA dataset in patients with high (n=129) and low (n=390) expression of *SFRP1* (Z< -1.5 is down-regulation and Z> 1.5 is up-regulation) in HNSCC patients.

TCGA: The cancer genome atlas, HNSCC: Head & neck squamous cell carcinoma, P values were generated using chi-squared analysis and the survival probability was plotted using Kaplan-Meier analysis.

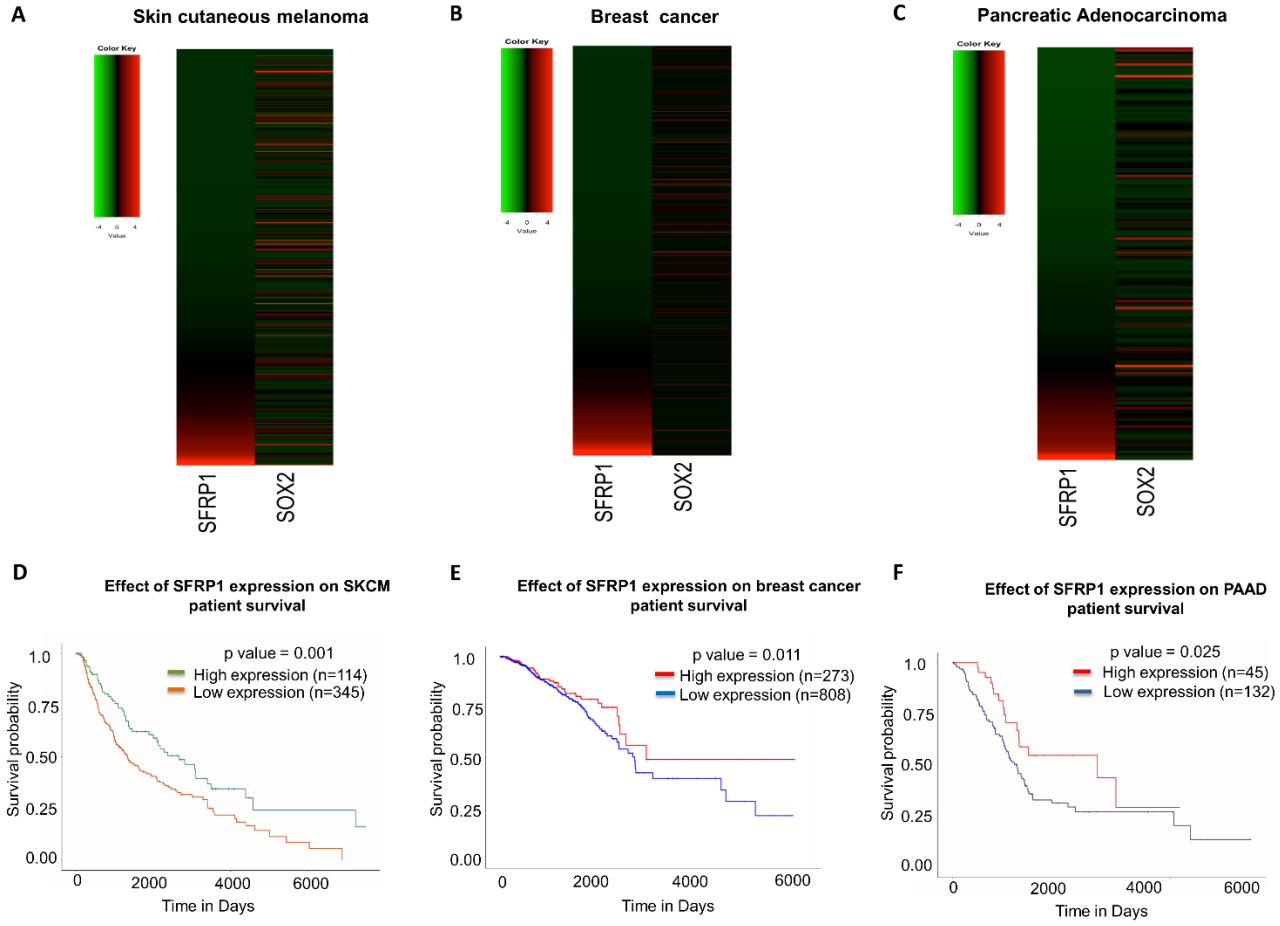

Figure S7: Decreased *SFRP1* expression and increase in *SOX-2* levels are observed in SKCM, breast cancer and PAAD patients (TCGA cohorts). Related to Figure 6.

A-C) Heat map of *SFRP1* and *SOX-2* expression in tumor samples showed inverse correlation among SKCM, breast and PAAD. Patients were sorted from *SFRP1* low to high expression (Z< -1.5 is down-regulation and Z> 1.5 is up-regulation) in SKCM, breast and PAAD respectively. Z scores were calculated as described in materials and methods

D-F) Survival analysis of TCGA dataset in patients with high and low expression of *SFRP1* (Z< -1.5 is down-regulation and Z> 1.5 is up-regulation) in SKCM (n=114 low and n=345 high), breast cancer (n=273 low and n=808 high) and PAAD patients (n=45 low and n=132 high). P-values were generated using chi-squared analysis.

SKCM: Skin cutaneous melanoma, PAAD: Pancreatic adenocarcinoma, TCGA: The cancer genome atlas, P values were generated using chi-squared analysis and the survival probability was plotted using Kaplan-Meier analysis.

Table S1: Real time PCR primers. Related to Figures 4, 5 & 6.

S.NO	GENE	Forward Primer (5'-3')	Reverse primer (5'-3')
1	*Snail*	GTCTGCACGACCTGTGGAA	CAGGAGAATGGCTTCTCACC
2	*E-Cadherin*	CAGCCTTCTTTTCGGAAGACT	GGTAGACAGCTCCCTATGACTG
3	*N-Cadherin*	ATGTGCCGGATAGCGGGAGC	TACACCGTGCCGTCCTCGTC
4	*Zeb1*	GCCAGCAGTCATGATGAAAA	TATCACAATACGGGCAGGTG
5	*Twist1*	AGCTACGCCTTCTCCGTCT	TCCTTCTCTGGAAACAATGACA
6	*Twist2*	CGCTACAGCAAGAAATCGAGC	GCTGAGCTTGTCAGAGGGG
7	*Nr2f1*	CCAGGCCAGTATGCACTCAC	CCGGGAAGAACGGGATGTT
8	*c-Jun*	AGCCTACCAACGTGAGTGCT	AGAACGGTCCGTCACTTCAC
9	*c-Fos*	GCCCAGTGAGGAATATCTGGA	ATCGCAGATGAAGCTCTGGT
10	*Sfrp1*	GACATCGGCTCGTATCAGAG	GTTGGGCAGCACCATCTTC
11	*Sox2*	CCTGGGCAGCGTGGCGGA	CAGACTGCGGGAAGAAGACG
12	*p21*	ATCCCGACTCTTGACATTGC	ACCCTAGACCCACAATGCAG
13	*Vimentin*	CGGCTGCGAGAGAAATTGC	CCACTTTCCGTTCAAGGTCAAG
14	*Keratin-8*	GGACATCGAGATCACCACCT	TGAAGCCAGGGCTAGTGAGT
15	*Wnt3A*	AATTTGGAGGAATGGTCTCTCGG	CAGCAGGTCTTCACTTCACAG
16	*Wnt7B*	ATCGACTTTTCTCGTCGCTTT	CGTGACACTTACATTCCAGCTTC
17	*Tgfβr3*	CATCTGAACCCCATTGCCTCC	CCTCCGAAACCAGGAAGAGTC
18	*Itgβ1*	AGTGCTCCCACTTCAATCTCAC	TCTCCTTGCAATGGGTCACAG
19	*SOX-2* human	GCCGAGTGGAAACTTTTGTCG	GGCAGCGTGTACTTATCCTTCT
20	*SFRP1* human	ACGTGGGCTACAAGAAGATGG	CAGCGACACGGGTAGATGG

Supplemental Experimental Procedures:

DMBA/TPA treatments:

The mice skin was shaved at postnatal day 22 (PD22) and topically treated with DMBA (9, 10-dimethyl-1, 2-benzanthracene) (50 μg/mice; 195 nM), which induces mutation in the Hras1 gene, for three times at PD23, PD25 and PD27. Further, TPA (12-O-tetradecanoyl phorbol-13-acetate), that enhances the proliferation of the epidermal cells which leads to clonal expansion of the mutated cells, was applied to the skin twice a week (2.5μg/ mice; 4 nM) for different time points. For papillomas, the mice were followed up to 6 months, and for SCC the mice were followed up to 10-12 months. The tumor growth was monitored and measured using digital Vernier calliper up to 12months at different time points.

Tumor collection and digestion for single cell suspension:

The tumors were collected in cold 1X Hanks balanced salt solution (HBSS) for further processing and tumor digestion. Tumor samples were minced in a solution containing 0.25% collagenase-I (Cat: C9891, Sigma) in HBSS and incubated at 37˚C for 1-1.5 hours on rocking plate. Collagenase-I activity was blocked by using EDTA (5mM) followed by 1X PBS containing 10% chelated FBS. The suspension was mixed thoroughly and then strained by using a 100μm strainer. The remaining tissue clumps were further digested by 0.25% trypsin (Cat: T4799, Sigma) at 37˚C for 10 min. The trypsin was neutralized with 10% chelated FBS in 1X PBS and passed through 70μm strainer. Cells were pelleted by centrifugation at 2000 rpm for 5 minutes and re-suspended in buffer containing 5% chelated FBS.

Isolation of CSCs from squamous cell carcinoma

The tumor samples were digested and single cell suspension was prepared as described above. CSCs were isolated by using well-defined markers such as $Lin^-/Epcam^+/\alpha6\ integrin^+/CD34^+$ from SCCs (Beck and Blanpain, 2013; Boumahdi et al., 2014; Lapouge et al., 2012; Schober and Fuchs, 2011). The cells of other lineages were excluded by using various antibodies conjugated with FITC such as CD45 (all hematopoietic cells except mature erythrocytes and platelets), CD31 (Endothelial cells) and CD140a (Fibroblasts). After preparation of the single cell suspension, cells were stained by using anti-mouse CD34 biotin (catalogue no:13-0341-85; eBiosciemce), anti-α6 integrin-PE (catalogue no: 555736; BD Pharmingen), anti-CD45-FITC (catalogue no: 103108, Biolegend), anti CD31-FITC (catalogue no: 102406, Biolegend), anti-CD140a-FITC (catalogue no: 11-1401-82, eBioscience), anti-Epcam-PE-Cy7 (catalogue no: 118216; Biolegend). Secondary antibody staining was performed by using streptavidin-APC (catalogue no: 554067; BD Pharmingen). The live cells were gated based on propidium iodide (PI) staining (catalogue no: P4170; Sigma). All the cells of other lineages were eliminated by using FITC gating as all the lineage specific antibodies used were tagged with FITC. Further the cells were gated for PE-Cy7 to select only Epcam positive cells. Then, the cells were gated using PE-Mouse IgG2a' k isotype control (catalogue no: 555574; BD Pharmingen) as anti-α6 integrin is conjugated to PE and with streptavidin-APC to eliminate cells with nonspecific

binding of secondary antibody streptavidin-APC. Fluorescence-activated cell sorting (FACS) and analysis was performed using FACSAria and FACSDiva software (BD Biosciences). Sorted cells were collected in lysis buffer for RNA extraction or into media for *in vivo* transplantation experiments.

Expression Profiling

RNA was extracted from the FACS sorted CSCs by using the absolutely RNA miniprep kit as described in the manufacturer's procedure (Cat: 400800, Agilent technologies). The RNA quality was assessed by Agilent RNA 6000 pico kit on the Agilent 2100 bioanalyzer. For microarray analysis, 1ng RNA was amplified by using the GeneChip® WT Pico amplification Kit (Affymetrix, USA) as per manufacturer recommendation. Further, 1 μg total RNA was reverse transcribed to cDNA with T7 Oligo d (T) primer (Affymetrix). The cDNA was used for in vitro transcription reactions containing T7 RNA polymerase. Then sense-strand cDNA was synthesized by the reverse transcription of cRNA using 2nd-Cycle Primers followed by RNase H hydrolyzes the cRNA template leaving single-stranded cDNA. The purified, sense-strand cDNA was fragmented by uracil-DNA glycosylase (UDG) and apurinic/apyrimidinic endonuclease 1 (APE 1) at the unnatural dUTP residues that break the DNA strand. The fragmented cDNA was labelled by terminal deoxynucleotidyl transferase (TdT) by using the Affymetrix proprietary DNA Labelling Reagent that is covalently linked to biotin. The fragmented and labelled product was loaded onto GeneChip® MTA 1.0 array (Affymetrix, USA) and was hybridized according to the manufacturer's protocol. Streptavidin-Phycoerythrin (Molecular Probes) was used as the fluorescent conjugate to detect hybridized target sequences. Raw intensity data from the GeneChip array were analyzed by GeneChip Operating Software (Affymetrix). The raw signal intensity data (.CEL files) obtained from the Affymetrix GeneChip® Command Console (AGCC) software were normalized and summarized using the RMA sketch algorithm implemented in Expression Console to generate normalized intensity data (.CHP files).

Real-Time PCR

Real-Time PCR (RT-PCR) reactions were performed by using Power SYBR green master mix (Kapa Biosystems) on Quant Studio 12K Flex Real-Time PCR System (Life Technologies). The Ct values were normalized by the expression level of β-Actin and GAPDH in respective samples. The fold change for relative expression of each target gene was calculated by using the $2^{-\Delta\Delta Ct}$ method. All the primers utilized are listed in supplemental information table S1.

H&E and Immunostaining on tumor sections:

For Immuno- fluorescence assay (IFA), the tumor sections were fixed using either acetone or 4% formaldehyde. The sections were then washed with 1x PBS and treated with 0.1% to 0.3% triton. Then blocking was performed using 5% NGS/NDS (normal goat serum & normal donkey serum) at room temperature for 1hr. After blocking primary antibody was added and the sections were kept overnight at 4^0C. On the second day the sections were washed (1X PBS) and treated with secondary antibody tagged with fluorophore for 1hr at room temperature. The sections were

then washed (1X PBS), treated with DAPI (4′, 6′-diamidino-2-phenylindole) and mounted with antifade before proceeding for imaging using LSM 780 confocal microscope (Zeiss).

For Immuno-histochemistry (IHC), the paraffin embedded tumor sections were deparaffinised and treated with either sodium citrate buffer (pH-6) or tris EDTA buffer (pH-9) for antigen retrieval. The sections were then treated for endogenous peroxidise activity and blocking was performed using 5% NHS (normal horse serum) at room temperature for 1hr. The primary antibody was added and then the sections were incubated overnight at 4^0C. The following day the sections were washed (1X PBST) and treated with biotinylated universal secondary antibody for 1hr at room temperature. The sections were then treated with freshly prepared avidin-biotin reagent and proceeded for DAB staining. The counter staining was performed using hematoxylin and the sections were mounted using DPX mountant (MERCK) and the images were acquired using upright microscope (Zeiss).

The Primary Antibodies used are Ki-67 (catalogue no: ab15580, Abcam), SOX-2 (catalogue no: ab92494, Abcam), VIMENTIN (catalogue no: ab92547, Abcam), KERATIN-8 **(**catalogue no: SAB4501654; Sigma**)**, KERATIN-5 (catalogue no: ab53121, Abcam), α6 INTEGRIN (catalogue no: 555734; BD Pharmingen) and SFRP1 (catalogue no: ab126613, Abcam). Secondary antibodies used were anti-rabbit Alexa Flour 568 (catalogue no: ab175471, Abcam), anti-rabbit FITC (catalogue no: 111-095-144; Jackson Immuno- research), anti-rat Alexa Flour 568 (catalogue no: ab175476, Abcam) and universal secondary antibody for IHC (catalogue no: PK-6200; Vectastain).

***In silico* analysis:**

To analyze the expression levels of *SFRP1* in normal and tumor samples of HNSCC, TCGA PANCAN normalized raw counts were obtained from UCSC cancer genome browser. These counts were transformed in (log2+1) values and represented between normal and tumor samples. Stage wise data was fetched from clinical data file of cBioPortal. Boxplot representation was performed in R 3.3.3 (http://www.R-project.org/). To see the correlation between *SFRP1* and *SOX-2* in tumor samples, Z scores were represented. Z scores for each tumor sample was calculated by subtracting the log2 normalized counts of each tumor sample from average mean log2 normalized count of normal samples and dividing that result by the SD of log2 normalized values of the normal samples. Heat map was also constructed using R 3.3.3 where Z-score >1.5 was considered as up-regulation and <-1.5 was considered as down-regulation. KMsurv package in R 3.3.3 was used to determine the correlation between overall survival in patients with high and low expression of *SFRP1*. The cut off values of Z-scores were used to identify patients with low v/s high expression levels and P values were determined using a chi-squared analysis. The similar protocol was followed for SKCM, breast and PAAD cancers.

cDNA synthesis and Real time PCR of *SFRP1* and *SOX-2* in human tissue samples:

Briefly, 2µg of isolated RNA was further treated with DNaseI (Fermentas) for 30 mins at 37^0C to degrade any possible DNA contaminant. DNaseI was inactivated by incubating the samples with 0.5M EDTA at 72^0C for 30mins. Purified DNase1 treated RNA was used for cDNA synthesis using RevertAid H-Minus first strand cDNA synthesis kit (Thermo Scientific RevertAid H minus First cDNA Synthesis kit, cat. K1632), according to the manufacturer's instructions. The obtained cDNA was prepared for RT-PCR reactions in triplicates in a 384-well

reaction plate. cDNA quality was determined by qPCR for house-keeping genes. In brief, cDNAs were then amplified with the corresponding gene-specific primer sets by PCR for 40 cycles using the condition of 30s at 94 ^{0}C, 60s at 60^{0}C followed by melt curve generation step. Real-time PCR mixture (5ul) contains 5 ng cDNA template, 2.5ul of SYBR GreenMaster Mix (Applied Biosystems), 0.2ul of each forward and reverse primer (10µM) and 1.9 µL RNase free water were added. The experiment was performed on applied Biosystems real time machine (QuantStudio12KFlex). ΔΔCt approach was used to calculate fold change. Seven breast tumor samples and six buccal mucosa samples were processed for analysis. Buccal mucosa samples were normalized with adjacent cut margin samples and breast samples were normalized with normal RNA purchased from Agilent (Cat: 540045).

Supplemental References

Beck, B., and Blanpain, C. (2013). Unravelling cancer stem cell potential. Nat Rev Cancer *13*, 727-738.

Boumahdi, S., Driessens, G., Lapouge, G., Rorive, S., Nassar, D., Le Mercier, M., Delatte, B., Caauwe, A., Lenglez, S., Nkusi, E.*, et al.* (2014). SOX2 controls tumour initiation and cancer stem-cell functions in squamous-cell carcinoma. Nature *511*, 246-250.

Lapouge, G., Beck, B., Nassar, D., Dubois, C., Dekoninck, S., and Blanpain, C. (2012). Skin squamous cell carcinoma propagating cells increase with tumour progression and invasiveness. EMBO J *31*, 4563-4575.

Schober, M., and Fuchs, E. (2011). Tumor-initiating stem cells of squamous cell carcinomas and their control by TGF-beta and integrin/focal adhesion kinase (FAK) signaling. Proceedings of the National Academy of Sciences of the United States of America *108*, 10544-10549.